L-Università ta' Malta

Department of Medical Physics
Faculty of Health Science

A Dissertation presented as part-fulfillment of the requirements for the award of the Masters in Medical Physics of the Faculty of Health Sciences of the University of Malta October 2024.

Dielectric measurements of skin cancer phantoms up to 50 GHz

Rodianne Sciberras

Supervisor: Prof. Lourdes Farrugia
Co-supervisor : Dr. Julian Bonello

Academic Year 2023/2024
MPH5008: Dissertation

L-Università ta' Malta

FACULTY/INSTITUTE/CENTRE/SCHOOL Faculty of Health Science

DECLARATIONS BY POSTGRADUATE STUDENTS

(a) Authenticity of Dissertation

I hereby declare that I am the legitimate author of this Dissertation and that it is my original work.

No portion of this work has been submitted in support of an application for another degree or qualification of this or any other university or institution of higher education.

I hold the University of Malta harmless against any third party claims with regard to copyright violation, breach of confidentiality, defamation and any other third party right infringement.

(b) Research Code of Practice and Ethics Review Procedures

I declare that I have abided by the University's Research Ethics Review Procedures. Research Ethics & Data Protection form code FHS-2023-00617.

As a Master's student, as per Regulation 77 of the General Regulations for University Postgraduate Awards 2021, I accept that should my dissertation be awarded a Grade A, it will be made publicly available on the University of Malta Institutional Repository.

For Mum and Aunty Lucy,

The two women who shaped who I am today through their love and guidance. I am eternally grateful to you.

For Andrei,

For being my forever best friend, who believed in me when I did not believe in myself.

Acknowledgments

I would like to extend my heartfelt thanks to the staff at the Electromagnetism Lab, particularly my supervisor, Professor Lourdes Farrugia, and co-supervisor, Dr. Julian Bonello. I am also deeply grateful to Dr. Iman Farhat and Mr. Federico Cilia for their support. This research would not have been possible without all their guidance.

I would also like to express my appreciation to Professor Carmel J. Caruana for his continuous support throughout the Master's program.

Special thanks go to the friends I have made along this journey, especially Mark Pickard- a Research Support Assistant at the Electromagnetism Lab, who offered tremendous assistance. I am also grateful to my friend, Kirsty Mangion, for making this academic journey more memorable.

None of this would have been possible without the support of those dearest to me. I am forever grateful to my mother Marisa and my siblings, Danica, Leonie, Ryan, Matthias, and Luca. And to Andrei Amaira and his parents, Isabel and Michael Amaira. Thank you all for believing in me when I could not believe in myself - you all have been my greatest inspiration.

Abstract

Background: Skin cancer is a global health issue. Non-invasive detection methods are crucial for early diagnosis, with microwave and millimetre-wave reflectometry offering potential due to their ability to differentiate between healthy and malignant tissues based on dielectric properties.

Objectives: The primary objectives were to develop phantom models that accurately represent the dielectric properties and anatomical features of the skin, tumour and fat tissues, extend the understanding of these properties into the millimetre wave spectrum, and assess the effect of the skin layer on tumour detection using dielectric spectroscopy.

Research Methodology: The research was conducted in four phases. Phase 1 involved familiarisation with dielectric measurements. Phase 2 focused on fabricating separate skin, tumour, and fat mimics. In Phase 3, two oil-in gelatin phantoms were constructed—one with an 8 mm fat layer embedding a 3 mm deep, 20 mm in diameter tumour, and another also including a 2 mm skin layer. Phase 4 evaluated tumour detection based on dielectric measurements and evaluated the effect of skin in detecting liposarcoma.

Results: Both phantoms accurately replicated the dielectric properties of human tissues. With the skin layer, detection was more challenging, particularly at higher frequencies, though the tumour was discernible in the real part of permittivity at lower microwave frequencies and in the imaginary part at higher millimetre wave frequencies.

Conclusions: Oil-in gelatin phantoms can accurately replicate dielectric properties of human skin, fat and tumours. While a skin layer reduced tumor clarity, detection was possible at specific frequencies.

Recommendations:: Further studies with varying skin thicknesses and higher frequencies are recommended for comprehensive analysis. Non-invasive technologies should be

prioritized for early cancer detection, and quality assurance protocols should address oil-in-gelatin phantoms' limited shelf life.

Keywords: Microwave reflectometry, millimetre waves, dielectric properties, oil-in gelatin phantoms, dielectric spectroscopy, skin cancer.

Contents

List of Acronyms x

List of Tables xiii

1 Introduction to the study 1

1.1 Introduction 1
1.2 Problem Statement 1
1.3 Background and Context 2
1.4 Objectives of the Study 4
1.5 Scope of the Study 5
1.6 Research Methodology 5
1.7 Ethical Considerations 6
1.8 Relevance to the study 6
1.9 Conclusion 7

2 Literature review 8

2.1 Introduction 8
2.2 Skin Cancer and its detection modalities 9
2.3 Effects of Electromagnetic radiation on biological tissue 11
2.4 Dielectric models for biological tissue 13

2.5 Electromagnetic modalities 16
2.5.1 Introduction 16
2.5.2 Microwave Reflectometry 18
2.5.3 Millimeter waves Reflectometry 21
2.5.4 Microwave Imaging 23
2.6 Measurement techniques 24
2.7 EM phantoms and their importance for Medical Physics 28
2.8 Conclusion 34

3 Research Methodology 36
3.1 Introduction 36
3.2 Research Approach 36
3.3 Research Methodology: Research Strategy 37
3.4 Research Methodology: Data Collection Technique 37
3.5 Research Methodology: Data Collection Procedure 38
3.5.1 Vector Network Analyzer and Open-Ended Coaxial Probe 38
3.5.2 Calibration Procedure 39
3.5.3 Phase 1: Familiarisation with Complex Permittivity Measurement Technique 40
3.5.4 Phase 2: Dielectric Measurements of Fat, Skin and Tumour Mimics for Phantoms 41
3.6 Research Methodology: Data Collection Tool 44
3.6.1 Outer casing of the oil-in-gelatin phantom: 44
3.6.2 Fabrication of the Oil-in-gelatin Phantoms: 46
3.6.3 Selection of Measurement for Dielectric Properties of the Fabricated Phantoms: 50
3.7 Data Analysis Technique 52

3.8 Pilot Study 54
3.8.1 Sunflower vs. Safflower oil for the Mimics 54
3.8.2 Outer casing for the oil-in-gelatin phantom 55
3.8.3 Fabrication of Coin-shaped Hollow for Tumour Mimic Insertion . . . 56
3.8.4 Grid for Dielectric Property Measurements 59
3.9 Ethical Considerations 60
3.10 Limitations of the Research Methodology 60
3.11 Conclusion 61

4 Results **62**
4.1 Introduction 62
4.2 Data 62
4.2.1 Phase 2: Dielectric Measurements of Fat, Skin, and Tumour Mimics . 62
4.2.2 Phase 3: Multilayer phantom fabrication and measurement of its dielectric properties 66
4.3 Data Analysis and Results 67
4.3.1 Phase 4: Dielectric maps for multi-layer phantom imaging 67
4.3.2 Additional Tests performed on Phantoms 70
4.4 Conclusion 76

5 Discussion **77**
5.1 Introduction 77
5.2 Discussion 77
5.3 Conclusion 90

6 Conclusions and Recommendations **91**
6.1 Introduction 91
6.2 Summary of Conclusions from the Study 91

6.3 Recommendations for Professional Practice 92
6.4 Recommendations for Future Research 93
6.5 Conclusion 94

References **95**

A Appendix **100**

List of Acronyms

BCC Basal Cell Carcinoma.

CT Computed Tomography.

dBm Decibel milliwatts.

E-field Electric field.

EIT Electrical Impedance Tomography.

EM Electromagnetic.

eV Electron Volt.

GHz Gigahertz.

ISM band Industrial, Scientific, and Medical band.

MHz Megahertz.

MMW Millimeter Wave.

MUT Material under Test.

MWI Microwave Imaging.

NaCl Sodium Chloride.

PETG Polyethylene Terephthalate Glycol.

RF Radiofrequency.

SCC Squamous Cell Carcinoma.

TMM Tissue-Mimicking Materials.

UWB Ultra-Wide Band.

VNA Vector Network Analyser.

List of Figures

3.1 Setup of the VNA, probe and the software used 39
3.2 Three-step calibration procedure 40
3.3 Ingredients used in the fabrication of the oil-in gelatin phantoms. From left to right: Kerosene oil, 200 Bloom Gelatin, deionised water (two separate bottles), p-toluic acid, sunflower oil (back), safflower oils (front), Propan-1-ol. 41
3.4 Photos taken during mimic fabrication 43
3.5 Outer casing design and dimensions created with Fusion 360 by Autodesk. 45
3.6 Fat mimic 46
3.7 Design of the coin-shaped hollow for the tumour insertion. 47
3.8 Schematic diagram for the creation of the coin-shaped hollow for tumour insertion. 48
3.9 Lab results for the creation of the coin-shaped hollow for tumour insertion. 48
3.10 Tumour mimic poured in phantom. 49
3.11 Skin mimic poured in phantom. 49
3.12 Dielectric properties of mimics in the oil-in gelatin phantoms 50
3.13 3D printed grid used for dielectric property measurements and its setup 51
3.14 Depth of probe in phantoms during measurements 53
3.15 Comparing lab results of tumour mimics (with Safflower oil and Kerosene, and Sunflower oil and Kerosene) with existing literature 54
3.16 Outer casing of oil-in gelatin phantom - Prototype 55

3.17 Coin-shaped hollow on the top of fat mimic for tumour mimic insertion - First approach 57
3.18 Coin-shaped hollow on the top of fat mimic for tumour mimic insertion - Second approach 58
3.19 Pilot study for grid 59

4.1 Comparison of laboratory results, shelf life, and reproducibility of skin mimic. . . . 63
4.2 Comparison of laboratory results, shelf life, and reproducibility of tumour mimic . 65
4.3 Comparison of laboratory results, shelf life, and reproducibility of fat Mimic. . . . 66
4.4 Oil-in-gelatin phantoms: from left to right—phantom with the skin mimic and phantom without the skin mimic 67
4.5 Dielectric properties at the surface of the oil-in gelatin phantom without skin mimic 68
4.6 Dielectric properties at the surface of the oil-in gelatin phantom with skin mimic . 69
4.7 Dielectric properties at 2.4 GHz - Phantom without the skin mimic. 70
4.8 Dielectric properties at 2.4 GHz- Phantom with the skin mimic. 70
4.9 Homogeneity test 1 71
4.10 The locations randomly chosen on the phantom without skin mimic 72
4.11 The locations randomly chosen on the phantom with skin mimic 73
4.12 The locations chosen for the variability in repeated measurements test . . . 74
4.13 Variability in repeated measurements test - Phantom without skin mimic . . 75
4.14 Variability in repeated measurements test - Phantom with skin mimic 76

5.1 Difference in dielectric properties between skin and tumour and skin and fat. 87

List of Tables

3.1 Parameters for 3D printing the outer case. 45
3.2 Parameters for 3D printing the outer casing prototype. 56

4.1 Assessment of the homogeneity of dielectric properties in the phantoms. 73

CHAPTER 1

Introduction to the study

1.1 Introduction

This chapter shall present the Problem Statement, Background and Context, Objective, Scope, Summary of the Research Methodology, Ethical Considerations, and Relevance of the Study.

1.2 Problem Statement

Microwave reflectometry techniques represent an active area of research in cancer diagnosis, particularly for breast and skin tumours [Kharkovsky and Zoughi, 2007]. Unlike some other diagnostic methods, microwave imaging is non-ionising and non-invasive, making it an intriguing field of study for the early detection of biological abnormalities [Kazemi et al., 2018]. The microwave frequency spectrum is between 300 MHz to 30 GHz [Kharkovsky and Zoughi, 2007].

Compared to microwaves, millimetre waves (MMWs) have higher frequencies, between 30 GHz to 300 GHz. Due to their higher frequencies, MMWs are less likely to penetrate deeply into the body and are primarily absorbed by the skin and superficial tissues [Mirbeik-Sabzevari and Tavassolian, 2019]. For frequencies higher than 300 GHz, the elec-

tromagnetic wave barely penetrates the skin [Kharkovsky and Zoughi, 2007].

The study by Boparai, J. and Popovic M. (2022) focused on testing the capabilities of microwave diagnostic tools to distinguish between healthy skin and lesions, in the frequency range of 0.5 - 26.5 GHz. To do so, phantoms were fabricated that accurately represent both the anatomical structure and the dielectric properties of human tissue [Boparai and Popović, 2022b].

This study aimed to extend the research conducted by Boparai J. and Popovic M. (2022) focusing on dielectric measurements conducted at higher frequencies ($>$ 26.5 GHz) within the millimetre spectrum. The measured data was used to infer some preliminary observations related to the imaging.

1.3 Background and Context

Skin cancer is a significant global health issue, with a specific focus on three primary subtypes: malignant melanoma (MM), basal cell carcinoma (BCC) and squamous cell carcinoma (SCC). BCC and SCC, categorised as non-melanoma skin cancer, are generally less aggressive than melanoma, but can still result in metastasis if not promptly diagnosed and treated. Timely detection is important for the effective management of all skin cancer types [Boparai and Popović, 2022a]. Healthcare professionals predominantly rely on a comprehensive visual examination protocol, guided by the ABCDE rule, which assesses various characteristics such as Asymmetry, irregular Borders, Colour variations, Diameter, and changes over time in skin lesions. Dermatoscopes and other specialised tools can also be used to improve the accuracy of identifying suspicious skin lesions; however, this method is somewhat subjective and prone to human errors [Boparai and Popović, 2022a]. A biopsy is generally needed in cases where the dermatologist suspects a tumour [Mehta et al., 2006].

Other alternatives for diagnosing skin cancers include the use of ionising radiation such as CT scans. Present literature highlights the need for a non-invasive and non-ionising skin cancer detection method [Mehta et al., 2006].

The potential of microwave reflectometry in the diagnosis of skin cancer lies in its non-ionising, non-invasive nature and cost-effectiveness [Kazemi et al., 2018]. It presents an opportunity to detect tumours in their early stages. Microwave reflectometry is a significant component of electromagnetic (EM) medical technologies. These technologies are particularly attractive due to their low cost and minimally invasive nature, which has led to extensive research efforts [Mehta et al., 2006]. The literature also states that using low-power microwaves for the diagnosis of skin cancer results in higher sensitivity and therefore promising detection of tumours in an earlier state [Boparai and Popović, 2022a].

This low-power microwave technique is based on examining differences in dielectric properties between normal and malignant tissues [Oliveira et al., 2018]. With this technology, the patient is irradiated with low-energy microwaves and the reflected signal is recorded. Compared to microwaves, millimetre waves have a shorter wavelength and thus penetrate less into the body. By analysing this reflected wave, information about the tumour can be extracted such as its shape and type [Oliveira et al., 2018]. Methods for converting the measured reflection coefficient to permittivity have been established over the years. Today, these processes are generally automated through software embedded in Vector Network Analysers (VNAs) [Oliveira et al., 2018].

The electrical properties of biological tissues influence how electromagnetic waves interact with them, affecting factors such as reflection, absorption, and transmission. These properties are also influenced by the frequency of the wave [Mirbeik-Sabzevari and Tavassolian, 2019]. The dielectric properties of biological tissues can be represented by their complex permittivity, denoted as ϵ_r, which describes how

the tissue interacts with an external electric field [La Gioia et al., 2018]. The most common mathematical models used to describe this electrical behaviour are the Debye, Cole-Cole, and Cole-Davidson models [La Gioia et al., 2018]. These models enable the determination of relative permittivity and conductivity values at a specific frequency [Mirbeik-Sabzevari and Tavassolian, 2019].

There are several ways to measure the dielectric properties of biological tissue, the most commonly used being the open-ended coaxial probe technique [La Gioia et al., 2018]. It offers several advantages including its simplicity, allowing for non-destructive measurements, and its broad frequency range.

For the successful evaluation of emerging microwave technologies in skin cancer diagnosis, the use of phantom models that replicate human tissues, both in terms of dielectric properties and within the frequency range of interest, is essential. Researchers use innovative techniques, including 3D printing, to develop phantoms that can be filled with tissue-mimicking materials to create accurate representations of human tissues [Boparai and Popović, 2022a].

1.4 Objectives of the Study

The objectives of the study were the following:

1. To delineate consistent heterogeneous phantom models that accurately depict both the dielectric properties and anatomical features of various skin, tumour and fat configurations.

2. To extend current knowledge of dielectric properties of skin up to 50 GHz to evaluate the dielectric properties in the millimetre wave spectrum.

3. To analyse the skin effect on producing images based on dielectric spectroscopy.

1.5 Scope of the Study

This study focused solely on one type of skin cancer, namely liposarcoma originating in the fat below the skin surface.

1.6 Research Methodology

The methodology for this research consists of four main phases:

1. **Familiarisation with Complex Permittivity Measurement Technique**:
   In the first phase of this study, a comprehensive understanding of the complex permittivity measurement technique was established. This involved conducting measurements on standard liquids such as ethanol and NaCl, allowing for proficient use of the open-ended coaxial probe and the VNA. This phase also included familiarising with mathematical models, such as the Cole Cole Model, which are essential for data interpretation. Subsequent steps included data analysis and comprehensive data reporting using both Python and Matlab.

2. **Fabrication and Dielectric Measurements of Fat, Skin, and Tumour Mimics for Phantom**:
   Skin, fat and tumour phantom mimics were fabricated separately as illustrated in the paper by Boparai, J. and Popovic M. (2022) and using an open-ended co-axial probe, their respective dielectric properties were measured up to a frequency of 50 GHz. This phase was essential prior to phantom fabrication to test the dielectric properties of the materials used to mimic skin, fat and tumour respectively as well as their repeatability and shelf life. For each phantom mimic, two subplots were obtained; Relative Permittivity against Frequency (GHz) and Imaginary Permittivity against Frequency (GHz).

3. **Multi-layer phantom fabrication and measurement of its dielectric properties**:

Oil-in-gelatin phantoms were fabricated using the tissue-mimicking materials analysed in phase two to simulate the dielectric properties of human tissues. The tumour was placed in the fat layer underneath the skin. Using an open-ended coaxial probe, the dielectric properties of the phantoms were measured. Using the probe, the reflection coefficients (S11) were measured and the VNA converted these S11 to the real (ϵ_r') and imaginary part (ϵ_r") of the complex permittivity (ϵ_r). It was made sure that before every reading, a standard three-load calibration was performed using air, a short block and deionised water, respectively.

4. **Dielectric maps for multi-layer phantom imaging:**

   The dielectric properties of the phantoms were measured at various locations across their surface at specific frequencies. The resulting spatial data was plotted and analysed, serving as a valuable visualisation tool for enhancing skin cancer diagnosis and imaging through dielectric spectroscopy.

1.7 Ethical Considerations

This research study focused on the measurement of dielectric properties within the specified frequency range and involved the use of phantoms as test subjects. It is essential to note that this investigation raises no ethical considerations, as it did not entail the participation of human patients or specific patient information.

1.8 Relevance to the study

The relevance of the study for the various stakeholders is as follows

1. **For patients**: To advance current technologies, for screening and imaging purposes as it uses non-ionising radiation.

2. **For physicists**: To gain better insights into the dielectric properties of tissue in the millimetre wave spectrum and how millimetre wave technology can be used in the medical sector.

3. **For the medical physicists**: This is an active area of research. Understanding the dielectric properties of tissues is essential for optimising EM imaging techniques for accurate diagnosis and treatment planning. This study also highlights the importance of using anthropomorphic phantoms.

1.9 Conclusion

This chapter presented an introduction to the study. Chapter two provides a critical review of the literature. Chapter three describes the research methodology, whilst chapter four presents the results. Chapter five provides an in-depth analysis and interpretation of the results. Chapter six summarises the most important conclusions of the study, proposes recommendations arising from the study, and suggestions for future research.

CHAPTER 2

Literature review

2.1 Introduction

The goal of this literature review is to briefly guide the reader through skin cancer and its detection modalities (Section 2.2), the effects of EM radiation on biological tissue (Section 2.3), dielectric models for biological tissue (Section 2.4), EM modalities (Section 2.5), measurement techniques (Section 2.6) and EM phantoms and their importance for Medical Physics (Section 2.7).

This review was initiated using the following electronic research databases: Google Scholar and HyDi. The following keywords were used (derived using the PICO framework where relevant): "microwaves, millimetre waves, skin cancer, oil-in gelatin phantoms".

Published papers in the last 35 years were considered (1987-2022). This was done as only a few papers were available related to the topic thus the search for literature had to be wider. An alert option was activated until the final submission date.

Selected articles had to satisfy the following inclusion criteria: (1) full-text papers and written in the English language, (2) studies that focus on medical physics applications, and (3) detection of tumours using microwaves. Duplicate findings were discarded to en-

sure that no data overlaps. The following criteria were then applied: (1) insufficient data, (2) inadequate methodology, (3) books and case study reports, and (4) subjective expert opinion papers. The article selection process was documented systematically using the Preferred Reporting Items for Systematic Reviews and Meta-Analyses (PRISMA); to illustrate a selection of studies for the review. Each article was analysed under the following themes: (1) title, author/s, year of publication, country of origin of the first author (2) research methodology, data collection tool, device name (3) sampling method, number of participants, response rate (4) findings (5) strengths and limitations of the study.

2.2 Skin Cancer and its detection modalities

The skin is the largest organ that covers the internal organs of the human body [Aminzadeh et al., 2014]. The epidermis, which includes the stratum corneum, the dermis, and the hypodermis, are the three main layers of tissue that make up the skin. The stratum corneum generally contains a higher proportion of water compared to the deeper layers, with its water content varying across different regions of the body [Topfer and Oberhammer, 2015]. Skin cancer stands out as one of the most common types of cancer [Aminzadeh et al., 2014]. Mehta et al. (2006) reported that annually, over one million individuals are diagnosed with skin cancer in the United States, with a mortality rate exceeding 1% each year [Mehta et al., 2006].

Despite the general perception of benign tumours as non-dangerous, some can lead to discomfort and serve as precursors to skin cancer. Malignant tumours, characterised by rapid duplication, cause metastases, destroying surrounding healthy tissues [Khuda, 2017]. There are three main types of skin cancer; Basal Cell carcinoma, Squamous cell carcinoma and melanoma. Early detection is important for the effective management of all skin cancer types [Boparai and Popović, 2022a]. This could be carried out clinically with the use of modern instrumentation [Khuda, 2017]. Visual inspection remains a common practice

in diagnosing skin cancers. A lesion's size, form, colour, abnormalities at the border, the presence of ulcers, its tendency to bleed, and whether or not it is elevated, firm or sensitive to the touch are all taken into consideration when making a diagnosis [Mehta et al., 2006].

However, this is prone to human error and somewhat subjective. Merkel cell Carcinoma, one of the least common types of skin cancer, is almost always misdiagnosed when relying only on visual inspection. Early-stage diagnosis enhances the curability of many skin cancers [Mehta et al., 2006].

In the case where cancer is suspected, dermatologists perform a biopsy. However, this method of detection is invasive and painful, thus the patient may require local anaesthesia. For this reason, there is an urgent need for non-invasive technologies that allow the early detection of skin cancer [Mehta et al., 2006]. Other diagnosis techniques include the use of ionising radiation such as a CT scan [Mehta et al., 2006]. This motivates researchers to design and develop non-invasive, non-ionising and cost effective diagnosis systems [Oliveira et al., 2018].

Research into the detection and treatment of various cancer types through non-ionising EM waves has been ongoing for several years. Microwave imaging techniques, in particular, have undergone thorough investigation in recent years [Mirbeik-Sabzevari and Tavassolian, 2018]. Microwave reflectometry shows potential for early skin cancer detection due to its non-invasive, non-ionising nature, as well as its cost-efficiency [Kazemi et al., 2018]. Literature also suggests that using low-power microwaves for skin cancer diagnosis enhances sensitivity, offering the potential for detecting tumours in the early stages [Mirbeik-Sabzevari and Tavassolian, 2018].

2.3 Effects of Electromagnetic radiation on biological tissue

The dielectric properties of tissues play a crucial role in governing the interaction of EM fields with the human body, influencing how EM waves are transmitted, absorbed, and reflected by biological tissues [La Gioia et al., 2018]. Dielectric characteristics serve as a measure of a material's ability to interact with EM energy [Khuda, 2017]. Since the pioneering research conducted by Foster and Schwan in 1980, the investigation into the dielectric properties of biological tissues has remained an ongoing field of research [Farrugia et al., 2016].

The EM radiation consists of both electrical and magnetic fields necessitating the consideration of electrical parameters such as conductivity and permittivity, along with magnetic parameters like magnetic permeability. However, for mammals, being non-magnetic, the magnetic permeability closely resembles that of free space [Pethig, 1987]. Hence when considering biological tissue, attention is focused solely on the relative permittivity and conductivity as these tissues do not exert a noticeable influence on the magnetic field itself. [Pethig, 1987]. In cases where EM waves traverse a uniform, lossless, and homogeneous material, dielectric properties are treated as real-number quantities. However, when the medium is characterised by losses and absorbs energy, the dielectric properties are derived from the measured relative complex permittivity [Khuda, 2017].

Interactions of biological tissue with an external electric field are defined by the complex permittivity ϵ^*, which can be mathematically described as:

$$\epsilon^* = \epsilon' - j\epsilon''. \tag{2.1}$$

The real part of the complex permittivity (ϵ') can be referred to as the dielectric constant. This factor describes the material's ability to store energy when exposed to an external E-field. The imaginary part of the complex permittivity (ϵ'') can be referred

to as the dielectric loss factor, indicating the dissipative nature of the biological tissue [La Gioia et al., 2018]. The conductivity (σ) is related to the imaginary part of the complex permittivity, and their relationship can be expressed through the equation below:

$$\epsilon'' = \frac{\sigma}{\epsilon_0 \omega} \tag{2.2}$$

where ϵ_0 is the permittivity of free space and ω is the angular frequency defined as $\omega = 2\pi f$, f being the frequency.

The relative dielectric permittivity provides insights into the tissue's ability to scatter the incident EM wave while conductivity reveals details about the signal loss as it propagates through the tissue. Higher conductivity correlates with increased loss attributable to attenuation and reflection. Research findings indicate a strong correlation between the relative electric permittivity of tissues and the presence of water; lower water content results in reduced permittivity, and conversely, higher water content leads to higher permittivity values [Khuda, 2017].

The application of an E-field results in charge displacement within the tissue, leading to dielectric polarisation [La Gioia et al., 2018]. The medium's response to a time-varying field is defined by the relaxation process, characterised by the exponential decay of polarisation in a dielectric medium after removing the applied E-field. A relaxation time '*t*' signifies the moment at which polarisation diminishes to *1/e* multiplied by its natural value, with '*e*' representing the base of the natural logarithm [Khuda, 2017].

The tissue's dielectric spectrum consists of three main dispersion regions; $\alpha-$, $\beta-$ and $\gamma-$ dispersion. Each dispersion reflects the behaviour of the tissue across various frequency ranges and contributes to the understanding of how energy is absorbed and dissipated in the biological medium. [La Gioia et al., 2018].

With an increase in frequency, the permittivity of biological tissues decreases due to dielectric relaxation. Within lower frequency ranges, specifically below 1 GHz, $\alpha-$ and $\beta-$relaxations occur, attributed to the presence of the cell membrane and boundaries. Another form of high-frequency relaxation, occurring at approximately 20 GHz, is identified as $\gamma-$ relaxation, linked to bound water. The Cole-Cole equation is used to describe the frequency-dependent relaxation characteristics of biological tissues by expressing complex permittivity as a function of frequency [Hwang et al., 2003]. The Cole-Cole equation will be further discussed in the next section.

2.4 Dielectric models for biological tissue

The complex permittivity of biological tissue is dependent on the frequency. This is due to the reduced ability of particles to quickly respond to rapid changes in the E-field, leading to a decrease in relative permittivity as frequency increases [Vorlıcek et al., 2010]. Tissue demonstrates multiple dispersions over a wide frequency range, primarily due to the dipolar relaxation behaviour of water molecules, which significantly affects its dielectric properties [Topfer and Oberhammer, 2015].

This dispersion spectrum is characterised by three main relaxation regions; $\alpha-$, $\beta-$ and $\gamma-$ at low, medium and high frequencies respectively, together with some other minor dispersions such as σ dispersion [Gabriel et al., 1996]. Each relaxation region denotes a distinct polarisation mechanism characterised by a single time constant, leading to the formulation of the complex relative permittivity. This process, known as dielectric relaxation, involves the gradual settling of sample polarisation towards a steady state, typically governed by a singular relaxation time constant (τ) [Gabriel et al., 1996]. The mathematical expression capturing this dielectric relaxation phenomenon is derived through the Debye relaxation equation, also referred to as the single Debye relaxation equation. This equation encapsulates the dielectric response of a substance when subjected to an external

electric field [Gabriel et al., 1996].

The Debye relaxation equation can be derived as follows:
The dielectric response of a MUT in an E-field can be given as:

$$\epsilon = \frac{D}{E} \tag{2.3}$$

where D is the electric flux density and E is the E-field strength.

Equation 2.3 can be rewritten as:

$$D = \epsilon_0 \epsilon_r E \tag{2.4}$$

The simplest form of relaxation process takes place as the material's polarisation approaches a stable condition and can be expressed by a single relaxation time constant, denoted as τ.

$$D = D_\infty + (D_0 - D_\infty)(1 - e^{-\frac{t}{\tau}}) \tag{2.5}$$

where,

- D_∞ is the electric flux density at high frequencies ($D_\infty = \epsilon_0 \epsilon_\infty E$)
- D_0 is the electric flux density at low frequencies ($D_0 = \epsilon_0 \epsilon_s E$)
- τ is the relaxation time varying from picoseconds to seconds according to the relaxation process.

Rewriting Equation 2.5, the following equation is obtained:

$$\epsilon_0 \epsilon_r E = \epsilon_0 \epsilon_\infty E + (\epsilon_0 \epsilon_s E - \epsilon_0 \epsilon_\infty E)(1 - e^{-\frac{t}{\tau}}) \tag{2.6}$$

Dividing Equation 2.6 by $\epsilon_0 E$:

$$\epsilon_r = \epsilon_\infty + (\epsilon_s - \epsilon_\infty)(1 - e^{-\frac{t}{\tau}}) \tag{2.7}$$

The Laplace transform can be performed to change from a time domain to a frequency domain:

$$\frac{\epsilon_r}{s} = \frac{\epsilon_\infty}{s} + \frac{(\epsilon_s - \epsilon_\infty)}{s} - \frac{(\epsilon_s - \epsilon_{\infty})}{s + \frac{1}{\tau}} \tag{2.8}$$

Multiplying by s, where $s = jw$ and rearranging, the following equation is obtained:

$$\epsilon_r = \epsilon_\infty + \frac{\epsilon_s - \epsilon_\infty}{1 + jw\tau} \tag{2.9}$$

Equation 2.9 is the well-known **Debye** equation, where ω is the anglar frequency.

Note that $\triangle\epsilon = \epsilon_s - \epsilon_\infty$, thus Equation 2.9 can be rewritten as:

$$\epsilon_r = \epsilon_\infty + \frac{\triangle\epsilon}{1 + jw\tau} \tag{2.10}$$

A conductivity term can be added to the Debye Equation to include the effect of current flow, as seen in Equation 2.11, where σ_s is the static conductivity.

$$\epsilon_r = \epsilon_\infty + \frac{\triangle\epsilon}{1 + jw\tau} - j\frac{\sigma_s}{\omega\epsilon_0} \tag{2.11}$$

The Cole-Cole model, different to the Debye model, includes the broadening of different dispersion regions by including an additional distribution parameter α

[Topfer and Oberhammer, 2015]. Equation 2.12 is the well-known **Cole-Cole** equation.

$$\epsilon_r = \epsilon_\infty + \frac{\triangle\epsilon}{1 + (jw\tau)^{(1-\alpha)}} - j\frac{\sigma_s}{\omega\epsilon_0} \tag{2.12}$$

The Debye and Cole-Cole models are commonly used to explain the electrical properties of biological tissues. These models, in conjunction with the **Havriliak-Negami relaxation**, provide a more comprehensive understanding by accounting for both the asymmetry and broadening of the dielectric dispersion curve [La Gioia et al., 2018].

$$\epsilon_r = \epsilon_\infty + \frac{\triangle\epsilon}{\left[1 + (jw\tau)^{(1-\alpha)}\right]^\beta} - j\frac{\sigma_s}{\omega\epsilon_0} \tag{2.13}$$

where α and β are the asymmetry and broadness parameters of dielectric dispersion respectively. When $\alpha = 0$ and $\beta = 1$, equation 2.13 results in the Debye Equation, while when $0 < \alpha < 1$ and $\beta = 1$ this corresponds to the Cole-Cole Equation.

In scenarios requiring the dielectric data of biological tissues, it has become needed to evaluate the permittivity and conductivity values using standard Debye and Cole-Cole models. These dielectric characteristics of biological tissues play an important role in the dissipation of electromagnetic energy within the human body.

2.5 Electromagnetic modalities

2.5.1 Introduction

The use of non-ionising EM waves for diagnosing and treating various cancer types has been a dynamic field of research [Mirbeik-Sabzevari and Tavassolian, 2018]. Challenges associated with ionising radiation, such as X-rays, have steered attention toward investigating diagnostic methods based on RF technology [Ruvio et al., 2013]. The field of med-

ical technologies using EM waves has experienced rapid expansion, serving dual roles in both diagnosis and treatment. The investigation into tissue-electromagnetic energy interactions holds significance not only for advancing electrical impedance imaging but also for broader medical domains, including RF and microwave-based diagnostics and treatments [Pethig, 1987]. These technologies, known for their cost-effectiveness and minimal invasiveness, have been a focal point for extensive research [Mehta et al., 2006].

Pathological alterations in tissue composition, particularly changes in water content, induce variations in dielectric properties that can be measured to discern physiological states aiding in diagnosis [Topfer and Oberhammer, 2015]. As highlighted by Topfer and Oberhammer (2015), a landmark conclusion in 1946 revealed that tumour tissue carries approximately 25% higher water content compared to healthy tissue. Metha et al. (2006) further emphasised that water content, whether in pure or bound form, significantly differs among normal, benign, and malignant tissues when assessing dielectric properties. Cancerous lesions manifest alterations in both water and salt content, and microwave signals interacting with tissues are responsive to these parameters, rendering them well-suited for cancer detection [Mehta et al., 2006]. Oliveira et al. (2018) demonstrated that backscattered waves carry crucial information about tumour shape and location. Typically, malignant tissues exhibit distinct dielectric properties that differ from those of surrounding healthy tissues, establishing an inherent dielectric contrast that can be detected [Mirbeik-Sabzevari and Tavassolian, 2018]. Therefore, a profound understanding of the dielectric properties of biological tissues is essential in EM medical technologies [Oliveira et al., 2018]. However, comprehensive dielectric data remains unevenly available for diverse tissue types, spanning various temperatures and frequencies.

In the next subsection, microwave and millimetre-wave reflectometry shall be discussed as promising techniques for the diagnosis and detection of cancerous tissue in the human body. The microwave frequency spectrum ranging from 300 MHz to 30 GHz, is

distinct from the millimeter wave spectrum, which ranges from 30 GHz to 300 GHz [Kharkovsky and Zoughi, 2007].

2.5.2 Microwave Reflectometry

Microwave reflectometry is a technique involving the use of microwaves to analyse the reflection electrical properties of various materials. It finds extensive application in the non-destructive assessment and characterisation of materials, such as biological tissues and metal structures, and crucial components of buildings and constructions [Kazemi et al., 2018]. This literature review specifically delves into the use of microwave reflectometry to analyse the reflection electrical properties of biological tissues, with a particular emphasis on skin tumour detection.

Numerous studies have explored the application of microwave reflectometry as a potential diagnostic method for the detection of tumours [Mehta et al., 2006]. In 2006, Mehta, P. et al. stated that while further research was required to comprehensively understand the reflection properties for both benign and malignant tumours and to establish the reliability of this means of diagnosis, the preliminary results showed potential [Mehta et al., 2006].

With microwave reflectometry, the tissue is radiated with low-energy microwaves, and the resultant reflected signal is recorded [Oliveira et al., 2018]. Various types of probes can be used in the microwave reflectometry process [Mehta et al., 2006]. The VNA plays a crucial role by generating a known incident wave, measuring both the incident and reflected signals, and providing a set of parameters known as S-parameters. S11, in particular, represents the reflection coefficient for a one-port device [Oliveira et al., 2018]. The measurement technique will be further discussed in Section 2.6. The measured reflection properties are directly impacted by the dielectric characteristics of the biological tissue [Kazemi et al., 2018]. The core concept of early tumour detection relies on investigating variations in dielectric properties between healthy and malignant tissues.

Studies state that backscattered signals vary depending on the presence of tumours of different shapes and sizes [Oliveira et al., 2018]. The levels of water, sodium, and protein differ between normal skin and both benign and malignant tumours, altering the dielectric properties of skin [Mehta et al., 2006]. Normal skin has a water content of approximately 60.9%, while malignant lesions display a higher content at 81.7%. Microwave measurements are expected to effectively identify these variations in water content. Additionally, malignant tissue typically possesses elevated sodium levels compared to normal skin, resulting in increased water retention and higher values of permittivity and conductivity [Mehta et al., 2006]. Thus, by measuring the reflection electrical properties at microwave frequencies, lesions can be differentiated from normal skin.

The study conducted by Mehta, P. et al. in 2006 used an open-ended coaxial probe and a frequency range of 300 MHz to 6 GHz, to measure the variations in dielectric properties between normal and moistened skin. This research focused on investigating the differences in reflection properties among skin, benign lesions, and malignant lesions, emphasising the role of water content when diagnosing tumours. This study aimed to demonstrate the potential of reflection properties as a foundation for diagnosing skin cancers. Experimental results concluded that differences in water content resulted in differences in reflection electrical coefficients, making microwave reflectometry ideal for the detection of skin cancer [Mehta et al., 2006].

In addition to variations in water content, Mehta, P. et al. (2006) investigated additional measurement parameters, including probe application pressure, power level, and the variation in skin reflection properties related to location and thickness. In the study, Mehta, P. et al. (2006) applied light pressure with the coaxial probe against the skin during measurements, ensuring adequate contact to minimise the possibility of air pockets forming between the tip of the probe and the skin. Three measurements at a single location were conducted with varying contact pressure, revealing that the measured reflection

coefficient remained consistent (within approximately 3%) across different pressure applications. This result suggested that as long as proper contact was ensured, variations in pressure did not significantly affect the measured reflection coefficient [Mehta et al., 2006].

The minimum power level needed for microwave reflectometry was also investigated, using power levels from -40 to 0 dBm. Even though, microwave signals are non-ionising, minimising power levels has its advantages including reducing local heat in the tissue. Below -40 dBm, variations in measured reflection coefficients became significant, approaching the limits of the equipment's capabilities. However, at -40 dBm and higher, differences among measurements fell within the expected range of uncertantiy. A power level of -30 dBm was adopted for all subsequent measurements in the study. This concluded that using power levels as low as -30 dBm results in accurate measurements of the reflected electrical properties of the skin. This study also indicated that the reflection coefficient measured is dependent on the thickness of the skin layer, causing variations in the reflection coefficients even for normal skin, depending on the body's location [Mehta et al., 2006].

Microwave reflectometry offers various advantages, including a low-power, real-time, and non-invasive method, coupled with high sensitivity. Its affordability, as a clinical system cost is a fraction of X-ray systems, renders it accessible for widespread screening. Importantly, the procedure poses no safety hazards, making it a viable and comfortable option for detecting even the smallest tumours in their early developmental stages [Kazemi et al., 2018]. In light of these findings, microwave reflectometry stands as a transformative approach with significant potential for advancing early tumour detection, contributing to more effective and accessible screening methodologies in the field of medical diagnostics.

2.5.3 Millimeter waves Reflectometry

The region of the EM spectrum between 30 and 300 GHz is known as millimetre waves (MMWs). Humans are consistently exposed to MMWs through diverse sources like 5G mobile communication systems [Mirbeik-Sabzevari et al., 2017]. The photon energy of MMWs, represented as hv (where h is Planck's constant and v is the frequency), falls within the range of 0.12 to 1.24 meV. Unlike ionising radiation, MMW photon energy does not disrupt molecular bonds, classifying MMWs as non-ionising. In addition, MMWs have an energy level lower than the thermal motion energy of about 0.025 eV. Only the energy associated with the orientational motion of molecular dipoles is lower than the photon energy of MMWs. Consequently, MMWs can engage with molecules possessing a rotational degree of freedom, such as water molecules. This interaction increases the thermal energy of water molecules, leading to molecular heating [Barnes and Greenebaum, 2018].

Expanding upon the non-ionising and interacting properties of MMWs, millimetre wave reflectometry emerges as a promising non-invasive diagnostic tool for tumour detection [Aminzadeh et al., 2014]. The skin, comprising about 70% water, becomes an intriguing subject for MMW reflectometry applications [Barnes and Greenebaum, 2018], particularly relevant for potential advancements in skin cancer diagnosis [Aminzadeh et al., 2014].

With a shorter wavelength, MMW have reduced penetration depth but offer higher spatial resolution [Mirbeik-Sabzevari et al., 2017]. Unlike terahertz, infrared, or optical frequencies, MMWs can still penetrate various layers of the skin but do not extend beyond the subcutaneous fat layer, in contrast to microwave reflectometry [Topfer and Oberhammer, 2015]. As mentioned by Topfer, F. et al. (2015) in their study, this presents an advantage over microwave reflectometry in skin cancer diagnosis, as it minimises signal interference from deeper tissues beyond the subcutaneous fat layer [Topfer and Oberhammer, 2015]. However, this makes MMW reflectometry less suitable for the detection of lesions placed deep within the body [Mirbeik-Sabzevari et al., 2017].

Like microwave reflectometry, this diagnostic tool relies on the difference in dielectric contrast between normal, benign and malignant tissue [Aminzadeh et al., 2014].

Compared to frequencies below 20 GHz, there is a dearth of information in the literature regarding the permittivity of human tissues at MMW frequencies, particularly those of the skin [Mirbeik-Sabzevari and Tavassolian, 2018]. The scarcity of dielectric property data for human skin at these frequencies is primarily attributed to the specialised and expensive instruments required for conducting measurements at such high frequencies [Aminzadeh et al., 2014].

The skin is the outermost layer of the body and thus understanding its dielectric properties is crucial for studies related to the potential interactions of MMWs with the human body [Topfer and Oberhammer, 2015]. This information serves to validate or refine existing standard models and forms the foundation for assessing the heat deposition and propagation of MMW signals within the body, providing valuable insights for safety considerations [Alabaster, 2003]. The study conducted by Gabriel et al. (1996) involved the assessment of dielectric properties in various tissues, including skin, with an extension into the MMW range, specifically up to 100 GHz. The dielectric data presented in the study were derived through extrapolation from measured data spanning 10 Hz to 20 GHz. This is acceptable as the extrapolation method is understood, yet the actual dispersions may or may not align with theoretical expectations [Aminzadeh et al., 2014].

In a subsequent study, Sasaki et al. (2014) used the measurements provided by Gabriel et al. (1996) as a reference, comparing them with their own in vivo measurements of dielectric properties in human epidermis and dermis within the frequency range of 500 MHz to 110 GHz [Farrugia et al., 2016]. The comparison revealed a good agreement between the two sets of dielectric properties up to 20 GHz. Beyond this frequency threshold, Sasaki et al. (2014) observed an increase in both dielectric constant (ϵ_0) and conductivity (σ) in their

measured data [Sasaki et al., 2014].

Additionally, Mirbeik-Sabzevari, A. et al. (2017), conducted a study measuring the dielectric properties of freshly excised normal and malignant skin tissues from skin cancer patients over a frequency range of 0.5- 50 GHz, obtaining slightly higher dielectric properties when comparing them to the widely used measurements from Gabriel et al. (1996) [Mirbeik-Sabzevari et al., 2017].

In conclusion, the integration of a diagnostic tool capable of enhancing patient throughput in skin cancer screening and improving diagnostic accuracy would be instrumental in detecting tumours before metastasis and reducing the need for unnecessary biopsies. Although visual inspection continues to be the primary method for diagnosing skin cancer, the incorporation of millimetre-wave technology could help fill gaps in the diagnostic process [Topfer and Oberhammer, 2015].

2.5.4 Microwave Imaging

Electrical Impedance Tomography (EIT) and Microwave Imaging (MWI) are EM imaging techniques, both renowned for their non-invasiveness and cost-effectiveness. MWI makes use of dielectric contrasts between different organs to distinguish between healthy and diseased tissues [La Gioia et al., 2018]. EIT has already found commercial success in lung-function monitoring applications while MWI has exhibited significant progress in clinical applications over the last two decades [La Gioia et al., 2018]. It exhibits promise in diverse medical scenarios, including breast cancer imaging, monitoring bladder volume for treating enuresis and urinary incontinence, and intracranial imaging for stroke detection [La Gioia et al., 2018].

A contemporary biomedical imaging technology, UWB MWI, is a compelling tool for the early detection of breast cancers. Operating in the frequency spectrum of 3.6-10.5 GHz,

UWB imaging relies on the transmission of very narrow pulses through tissues, penetrating a targeted area, with reflections and scattering signals received by a UWB antenna, providing crucial information. Signal processing techniques such as beamforming, hypothesis testing, and time-reversal imaging are then used to detect and localise different scattering regions [Khuda, 2017].

The primary focus of MWI and associated signal processing algorithms has been the detection of tumours within the breast [Oliveira et al., 2018]. This modality has expanded its applications to characterise biological abnormalities, including skin cancer, as well as skin burn injuries. A study conducted by Kazemi, F. et al. (2018) proposed MWI systems for skin abnormalities, such as a 13.5 GHz microwave sensor designed for near-field imaging of skin abnormalities. The sensor demonstrated the ability to diagnose both visible and hidden abnormalities, positioning it as a promising low-cost solution for rapid and precise skin cancer detection [Kazemi et al., 2018].

2.6 Measurement techniques

Various methods have been developed to evaluate the dielectric properties of biological tissues, each with its own set of advantages and limitations. The transmission line, the resonant (cavity) method, the free space, and the open-ended coaxial probe methods are some of these techniques [La Gioia et al., 2018]. Every measurement method is constrained by the particular frequencies, materials, and applications for which it is designed. Understanding these limitations is crucial for selecting the most appropriate method that aligns with the specific objectives of the research [Venkatesh and Raghavan, 2005]. The open-ended coaxial probe technique stands out as the most commonly used method in current research [La Gioia et al., 2018].

a. Transmission Line Method:

In the transmission line measurement method, the MUT is placed in a coaxial line or a rectangular waveguide, allowing for variation of field polarisation. The transmission line is connected to a VNA to measure the complex scattering parameters. These parameters include the reflected signal (S11) and the transmitted signal (S21), which are evaluated to obtain the complex permittivity and permeability of the material, representing the dielectric properties of the tissue [La Gioia et al., 2018]. This method offers several advantages, particularly its suitability for samples with medium to high loss, providing a means to measure both the permittivity and permeability of the material under investigation. Although the transmission line method allows measurements across a broad frequency range, its application is restricted to low temperatures [Venkatesh and Raghavan, 2005]. Furthermore, the accuracy of measurements can be affected by the presence of air gaps [La Gioia et al., 2018].

b. Resonant (Cavity) method:

The resonant cavity measurement method stands out as one of the most accurate methods for measuring both the permittivity and permeability of MUT. Among the most widely used resonant techniques are perturbation methods, which are suitable for various permittivity measurements as well as for testing magnetic and medium-to-high-loss materials. For low-loss materials, a larger sample size is required to ensure accurate results. The resonance characteristics of the MUT within the cavity include its quality factor (Q) and the resonance (centre) frequency (f). These characteristics are measured to determine the dielectric properties (ϵ_r and μ_r) of the MUT. This is done by comparing the resonant frequency and quality factor of an empty cavity with the same measurements after the MUT is introduced. A distinct advantage of this method is that it does not require network analyser calibration, making it simpler in practice. It is especially useful for small MUT samples, though it requires a high-

frequency resolution VNA and is generally limited to a narrow band of frequencies. [Venkatesh and Raghavan, 2005].

c. Free space method:

The free space method consists of a network analyser, which needs to be first calibrated, attached to two antennas that are positioned facing each other. First, the S-parameters of an empty sample holder, positioned mid-way between the antennas, are determined. The MUT is then placed in the sample holder, and the S parameters are again measured. The S-parameters include both the reflection and transmission coefficients. Using the insertion feature of the VNA, it becomes possible to eliminate the effect of the sample holder, allowing determination of the S-parameter of the MUT. The measured reflection and transmission coefficients are then post-processed to determine the dielectric properties of the material (ϵ_r and μ_r). The free space method is suitable for high-frequency measurements and in hostile environments. However, this technique includes potential multiple reflections between the antenna and the sample surface [Venkatesh and Raghavan, 2005].

d. Open-ended coaxial probe method:

This method consists of an open-ended coaxial probe, which is a truncated section of a transmission line, and a VNA, which needs to be first calibrated. The VNA emits an E-field through the coaxial probe which results in reflection if there is an impedance mismatch between the probe and MUT. By comparing the incident and reflected signal (S11 parameter), the VNA determines the permittivity of the MUT. In this method, the probe is either pressed against the MUT or submerged in liquids, measuring the reflection coefficient to derive the permittivity [La Gioia et al., 2018]. This technique allows contact between the probe and the sample without significantly altering the material's characteristics and minimal sample preparation. This method is suitable for

semi-solids.

To ensure accurate and reliable measurements with the open-ended coaxial probe, certain precautions must be taken. The probe cable should be immobilised to eliminate any risk of bending, and the electrical connectors should be properly secured [Alborova et al., 2017]. The advantages of the open-ended coaxial probe method are significant, requiring no machining of the sample and allowing for rapid measurements of dielectric properties in a temperature-controlled environment after calibration. However, limitations include its reliance on reflection measurements only and its susceptibility to air gaps during the measurement process [Venkatesh and Raghavan, 2005].

Numerous studies considered in this literature review have used the open-ended coaxial probe technique together with a VNA to assess the complex reflection coefficient (S11 parameter). In their research, Alborova et al. (2017) stated that the S11 parameters obtained are converted to complex permittivity using Agilent 85070E software. Similarly, the study conducted by Farrugia et al. (2016) used Agilent 85070E software to convert the measured S11 parameters into dielectric properties. Technological advances have facilitated the integration of software programmes with these techniques, facilitating the measurement process for complex reflection and transmission coefficients using a VNA [Alborova et al., 2017].

Before commencing measurements, it is essential to set up measurement parameters including setting up the appropriate frequency range and the number of measurement points. Subsequently, the calibration of the probe becomes a critical step in the process [Alborova et al., 2017].

As Farrugia et al. (2016) stated in their research, the calibration process involved measuring the complex reflection coefficient under three standard conditions: when the probe is

short-circuited, when the probe is radiating into air (open circuit), and when the probe is radiating into a reference liquid (deionised water) with known dielectric properties. Gabriel and Peyman (2006) emphasised the importance of accurate knowledge of the dielectric properties of the calibration liquid, not only for calibration verification but also to estimate systematic errors. To minimise measurement errors related to cable shape changes, the cable was fixed in the calibration position, while the MUT was moved for each measurement [Farrugia et al., 2016].

2.7 EM phantoms and their importance for Medical Physics

Phantoms play a crucial role in medical physics and biomedical engineering, including their use in clinical settings for quality control and the validation of medical devices and technologies used in both diagnosis and treatment [Khuda, 2017]. Phantoms ensure that medical devices and technologies are up to standards according to European protocols, minimising any risks to patients and ensuring the highest standard of healthcare delivery [Chahat et al., 2012].

Similarly, for research and development purposes, in comparison to numerical models, anthropomorphic phantoms provide tangible, and physically accurate representations of human tissues and physiological conditions in a controlled environment [Joseph et al., 2020]. Phantoms help to evaluate the interaction of EM fields with human tissue, making them beneficial when evaluating the performance and safety of microwave-based medical devices [Mirbeik-Sabzevari and Tavassolian, 2018]. Thus, the development of anthropomorphic phantoms helps in accurate, reproducible and controlled experiments for the assessment of medical devices and technologies [Boparai et al., 2020].

Despite all the advancements, challenges are still present when fabricating anthropomor-

phic phantoms, especially when these phantoms are to be used over a wide frequency spectrum [Ruvio et al., 2013]. When developing anthropomorphic phantoms to be used in microwave reflectometry one should consider the relaxation time and its frequency dependence, to obtain accurately characterised permittivity and conductivity measurements [Khuda, 2017]. This means that the phantom's dielectric properties should change with changing frequencies. For this reason, the choice of material is crucial when developing such a phantom [Khuda, 2017]. Khuda, I.E. et al. (2017) state the importance when developing these phantoms, taking into account factors such as the desired measurements needed, the long-term stability of mechanical and EM properties [Joseph et al., 2020] and geometric considerations [Boparai et al., 2020]. The shelf life of a phantom should be assessed [Khuda, 2017]. Joseph, L. et al. (2020) also state that besides the dielectric properties of human tissue, these phantoms need to reflect the physical and anatomical structure to obtain realistic results [Joseph et al., 2020].

Anthropomorphic phantoms can be fabricated in either solid, liquid or semisolid states [Mirbeik-Sabzevari and Tavassolian, 2018]. Solid phantoms are typically made from ceramic powders or chemically synthesised polymers like silicone or polyvinyl chloride. However, studies indicate that solid phantoms may not accurately mimic the dispersive properties of biological tissue across a broad frequency range. Liquid phantoms are easily fabricated however long-term stability is difficult to maintain as they tend to dehydrate, leading to changes in the relative permittivity and conductivity of the phantoms [Mirbeik-Sabzevari and Tavassolian, 2018]. Semi-solid phantoms, which are water-based, offer various advantages over solid and liquid phantoms. Some of these advantages include their ability to conform to any shape, allowing for multi-layered phantoms since no osmosis occurs. These phantoms can mimic realistic situations of soft tissue. The two main components of a semi-solid phantom are water and solidifying agent that gives it a jelly-like consistency. The most used semi-solid phantom when fabricating skin is the

oil-in gelatin phantom which is proven to mimic well the dielectric properties of skin tissues over a broad range of frequencies. Gelatin is a gel-like substance made from natural collagen found in sources like porcine skin. Most literature on oil-in-gelatin phantoms is limited to microwave frequencies [Mirbeik-Sabzevari and Tavassolian, 2018].

In the literature reviewed, no studies were chosen that specifically addressed the fabrication of liquid phantoms to mimic human tissue properties. However, two studies focusing on solid phantoms were identified. In one study conducted by Garrett, J. and Fear, E. (2014), mixtures consisting of graphite, carbon black, and urethane were fabricated to evaluate their dielectric properties. The study showed that these composite materials have a wide range of dielectric properties, suitable for mimicking various soft tissues. Particularly, the materials were found to be well-suited for constructing skin layers, offering thin, flexible, and robust structures. For this study, a flexible and mechanically strong tissue-mimicking material (TMM) was required. Consequently, a carbon-based conductive filler and a rubber matrix (both silicone and urethane rubber were tested) were chosen. The findings indicated that an increase in the concentration of graphite resulted in higher dielectric properties of the phantom. Modifying the carbon powder concentration allows TMM to demonstrate a broad spectrum of dielectric properties, simulating various human soft tissues across the frequency range of 1 to 10 GHz [Garrett and Fear, 2014]. The study by Boparai, J. et al. (2020) also makes use of carbon black, polyurethane and graphite to mimic skin tissue. This study also states that by varying the ratio of concentrations in these three materials, different dielectric properties can be obtained. This phantom type demonstrated stability over several months and was evaluated within the frequency range of 5 to 20 GHz. This phantom was reported as a suitable model of human skin [Boparai et al., 2020].

Three studies examined the fabrication of semi-solid breast phantoms, each using oil-in-gelatin phantoms to mimic breast tissue using a combination of everyday chemicals.

Joseph, L. et al. (2020) developed a comprehensive breast phantom consisting of four tissue types: skin, fat, muscle, and tumour, while Porter, E. et al. (2010) focused on gland tissue instead of muscle. In their study, Porter, E. et al. (2010) emphasised the need for low-cost, off-the-shelf materials that remain stable over time. Both Ruvio, G. et al. (2013) and Porter, E. et al. (2010) observed that adjusting the oil concentration, composed of 50% kerosene and 50% safflower oil, allowed variation in the phantom's dielectric properties, allowing the chosen materials to have a wide range of dielectric properties depending on the concentrations used. The breast phantom developed by Joseph, L. et al. (2020) included tumour inclusions of various sizes (4 mm, 8 mm, 16 mm) inserted into the fat tissue, with the S21 parameter evaluated across a frequency range of 0.5 to 20 GHz. Using an oil-in-gelatin phantom, they fabricated a multilayered and adjustable model. The mold for the phantom was designed using CAD Fusion 360 and 3D printed with ABS filament. The primary objective of this research was to determine the minimum detectable tumour size using non-invasive microwave transmissions. Results indicated that tumours as small as 4 mm in diameter could be detected using microwave technology, suggesting promising advancements in non-invasive breast cancer detection techniques. Ruvio, G. et al. (2013) concluded that oil-in-gelatin phantoms can replicate the electrical properties of both normal and malignant breast tissue.

The study conducted by Porter, E. et al (2010) details the three main steps taken to construct the breast phantom. The first step is the fabrication of the individual tissue phantoms - fat, gland, skin and tumour using readily available ingredients: p-toluic acid, n-propanol, deionised water, 200 Bloom gelatin, Formaldehyde, oil (50% safflower oil and 50% kerosene) and Ultra Ivory detergent. Careful selection of ingredients ensured the production of stable phantoms with prolonged storage capabilities. The second step included the measurement of the dielectric properties of each tissue phantom after they were allowed to solidify. This was done using an HP 85070B dielectric probe together

with a VNA. The dielectric properties of the skin phantom were the most accurate when compared to actual skin tissue. The final step consisted of fabricating the complete breast phantom. This was achieved by amalgamating the four tissue phantoms into a cohesive model mimicking human breast anatomy. However, this phase posed challenges, particularly in preventing the formation of air pockets within the phantom. The skin was set first and time was allowed for it to solidify. The fat was then poured directly into it. Tumour models were also placed at different locations within the fat [Porter et al., 2010].

Joseph, L. et al (2018) fabricated a low-cost semi-solid phantom to mimic human skin. The phantom's size and thickness were determined based on the average thickness of human tissue. The skin phantom was fabricated using deionised water, corn flour, kerosene, TX-151, salt and benzoate. Despite skin being a tissue with high water content, the water content in the phantom was minimised to ensure malleability and long-term preservation without changing its electrical properties. Kerosene was the main ingredient used to adjust the permittivity of the phantom. The combination of corn flour and TX-151 produced a flexible and moldable texture. Sodium benzoate acted as a preservative, while salt was added to regulate the conductivity. The fabrication procedure involved mixing deionised water and corn flour until combined. The mixture was then boiled, with kerosene gradually added while continuing to boil. The heating was stopped once the kerosene was well incorporated into the mixture. Salt and sodium azide were then added. TX-151 was slowly added to the stirred liquid, with stirring continued until the viscosity of the mixture increased. The resulting mixture was poured into a mold and allowed to cool at room temperature for several hours until solidified. Once the phantom was fabricated, its dielectric properties were measured using an open-ended transmission line between a frequency range of 500 MHz to 20 GHz. This study concluded that the dielectric measurements obtained using this skin phantom closely matched the real and imaginary part of the complex permittivity for human dry skin, owing to the absence of water and agar-

based ingredients in the phantom [Joseph et al., 2018].

The study conducted by Chahat, N. et al. (2012) aimed to develop a skin phantom that can accurately mimic the dielectric properties of human skin in the millimetre frequency range, up to 65 GHz. The main ingredients used to fabricate this phantom were deionised water, agar, polyethene powder, TX-151 and sodium azide. The polyethene powder was used to change the real and imaginary parts of the phantom's permittivity. This study highlighted the importance of maintaining a constant room temperature throughout the whole phantom fabrication. Chahat, N. et al. (2012) also emphasised the necessity of preventing water evaporation to preserve the dielectric properties of the phantom for longer periods. To verify the accuracy of this phantom, evaluations of specific absorption rates were conducted at 60 GHz. The findings exhibited a strong agreement between the experimental results and numerical predictions. The dielectric properties of the phantom were assessed using a coaxial probe and subsequently compared to the in-vivo dielectric properties of human tissue measured before the fabrication of the phantom, showing excellent agreement between the two [Chahat et al., 2012].

The study by Mirbeik-Sabzevari, A. and Tavassolian, N. (2018) also fabricated skin-equivalent semisolid phantoms to be used for millimetre wave reflectometry. Healthy and malignant skin tissues were replicated individually using suitable mixtures of deionised water, oil, gelatin powder, formaldehyde, TX-150 (gelling agent) and detergent. TX-150 was used to enhance the longevity of the phantom by increasing its viscosity. However, this nonionic surfactant had the drawback of reducing dielectric permittivity. To counteract this effect, NaCl was introduced to increase the conductivity, particularly for frequencies below 25 GHz. Meanwhile, the detergent functioned as an emulsifier, ensuring the even dispersion of oil within the water-based solution to create uniform oil-in-water emulsions [Mirbeik-Sabzevari and Tavassolian, 2018].

The dielectric characteristics of these phantoms were assessed across frequencies ranging from 0.5 to 50 GHz using an open-ended coaxial probe together with a millimetre-wave VNA. Cole-cole model was then used to fit the complex permittivity data. The permittivity measurements obtained showed good agreement with the permittivity values determined from fresh skin samples obtained ex vivo. Furthermore, the depth to which millimetre waves penetrate normal and malignant skin phantoms was calculated. The analysis showed that these waves were able to penetrate the human skin sufficiently to interact with most of the structures within the epidermis and dermis layers [Mirbeik-Sabzevari and Tavassolian, 2018].

Dielectric measurements were made at four different depths in the phantom to examine the homogeneity of it. Results showed that the reflection coefficients decreased as the probe penetrated deeper into the phantom, indicating higher absorption in the deeper layers. The maximum difference between the top and bottom surfaces was approximately 25 dB (at 37 GHz). This difference was mainly due to the gravitational migration of water towards the bottom of the phantom after some time. Measurements taken after three days demonstrated that the reflection coefficients stabilise as water migration saturates. To assess the reproducibility of the fabrication procedure, a set of ten samples for each of the three skin-simulating phantoms was produced over a ten-day period. Measurements were conducted on each sample at an identical depth three days post-fabrication. The stability of the phantoms was evaluated by measuring the three types of phantoms for up to 30 weeks after fabrication [Mirbeik-Sabzevari and Tavassolian, 2018].

2.8 Conclusion

This literature review has examined the advancements and limitations in current skin cancer detection techniques and electromagnetic interactions with biological tissues. The following conclusion summarises the key research gaps identified and links them to the

primary objectives of this study.

Current methods for skin cancer diagnosis often involve invasive procedures or reliance on ionising radiation, which can carry health risks and be costly. While effective, approaches like biopsies and CT scans underscore the need for safer, non-invasive diagnostic alternatives. Additionally, research on dielectric properties beyond 26.5 GHz is limited, leaving a gap in understanding skin and tumour tissue electrical behaviours in the MMW range. This gap is significant, as MMWs allow for shallow penetration, which is suitable for skin-level diagnostics, and may enhance the contrast between healthy and malignant tissues, supporting early detection.

Another challenge is the absence of consistent, multilayer phantoms that closely replicate the dielectric and anatomical characteristics of skin, fat, and tumour tissues across broad frequency ranges. The lack of such phantoms limits the ability to conduct reliable, clinically relevant experiments that accurately mimic in vivo conditions. This study expanded on the research conducted by Boparai and Popovic (2022).

Furthermore, there is minimal research on how the dielectric properties of the skin layer influence imaging using dielectric spectroscopy. This effect is crucial, as higher frequencies within the MMW spectrum may face limitations in penetrating deep-seated tumours. The skin's high permittivity and conductivity, similar to that of tumour tissue, complicate tumour detection, reducing dielectric contrast. Evaluating the role of the skin layer in dielectric-based imaging is essential to determine if sufficient penetration and contrast are achievable for reliable tumour detection. This study addresses this gap by analysing permittivity maps, which provide visual representations of the dielectric variations within the phantom models, to assess the impact of the skin layer on image clarity and tumour detectability.

CHAPTER 3

Research Methodology

3.1 Introduction

This chapter presents the research methodology used in the study. This includes the Research Approach, Research Strategy, Data Collection Technique, Data Collection Procedure, Data Collection Tool, Data Analysis Technique, Pilot Study, Ethics Considerations and Limitations of the Research Methodology.

3.2 Research Approach

This research project used a quantitative research design. The methodology was divided into four main phases to ensure thorough investigation and validation of the techniques used. The first phase involved familiarising with complex permittivity measurement techniques. This process included the calibration of the VNA and mastering the proper use of the open-ended coaxial probe. To establish a baseline understanding and accuracy, measurements were conducted on standard liquids, specifically NaCl and ethanol.

In the second phase, attention was focused on the fabrication and dielectric measurement of fat, skin, and tumour mimics. These mimics were fabricated to accurately simulate the dielectric properties of human tissues. This phase was essential for constructing a realis-

tic phantom model, aimed at emulating the dielectric properties of human skin, fat and tumour. This phase was critical for ensuring that the phantom would provide reliable data in the study's experimental procedures. The third phase of the methodology was dedicated to the fabrication of the oil-in-gelatin phantoms. This step involved carefully combining the prepared mimics to form a composite material that closely replicates the dielectric properties of human tissues. The resulting phantoms served as a model for conducting experiments to assess the potential for detecting skin tumours using microwaves.

Finally, the fourth phase encompassed data analysis and dielectric measurements of the fabricated phantom. This phase aimed to evaluate the effectiveness of using microwaves and millimetre waves in detecting skin tumours based on the dielectric properties of the constructed model. The comprehensive analysis provided insights into the potential of these techniques for non-invasive medical diagnostics.

3.3 Research Methodology: Research Strategy

The research strategy used in this study was experimental, aimed at investigating the dielectric properties of skin cancer phantoms from 500 MHz to 50 GHz. The fabrication of phantoms required careful calibration and validation processes, which were best supported by an experimental framework. The study was conducted prospectively, involving the design, execution, and real-time analysis of experiments to measure the dielectric properties of the phantoms.

3.4 Research Methodology: Data Collection Technique

The data collection technique used in this study was primarily based on direct measurements using specialised equipment. The open-ended co-axial probe method, in conjunction with a VNA was used to measure the dielectric properties of the phantoms. The

choice of this data collection method was driven by its ability to provide accurate and rapid measurements across a broad frequency range. The open-ended coaxial probe method was selected for its ability to measure complex permittivity with minimal sample preparation, ensuring that the dielectric properties of the phantom remain unchanged. This was crucial for meeting the study's objectives.

3.5 Research Methodology: Data Collection Procedure

3.5.1 Vector Network Analyzer and Open-Ended Coaxial Probe

In this study, the Rhode and Schwarz ZVA-50 VNA was used to conduct all measurements. The ZVA-50 VNA is capable of operating within a frequency range of 10 MHz to 50 GHz, providing high precision and accuracy essential for complex permittivity extraction. This apparatus was selected for its robustness and advanced features, which include multiple ports and extensive frequency coverage, which make it suitable for a wide range of EM measurements [Keysight Technologies, 2020].

The primary parameter measured was the S11 reflection coefficient, which represents the complex reflection of the signal at the probe interface. This parameter was crucial in determining the complex permittivity of various samples. The data collected by the VNA was processed using the Keysight 85070E software, which is specifically designed for dielectric material measurements. The software facilitated the accurate extraction of permittivity values by analysing the S11 parameter and applying the necessary mathematical models.

Complementing the VNA, the probe was used for its capability to perform non-destructive testing on samples. Its design allows it to interface directly with the MUT, ensuring minimal perturbation of the sample, while also enabling wideband measurements from 500 MHz up to 50 GHz.

The combination of the Rhode and Schwarz ZVA-50 VNA and the probe (Figure 3.1),

provided a robust setup for the study, ensuring high accuracy and repeatability in the measurements of complex permittivity across a broad frequency range.

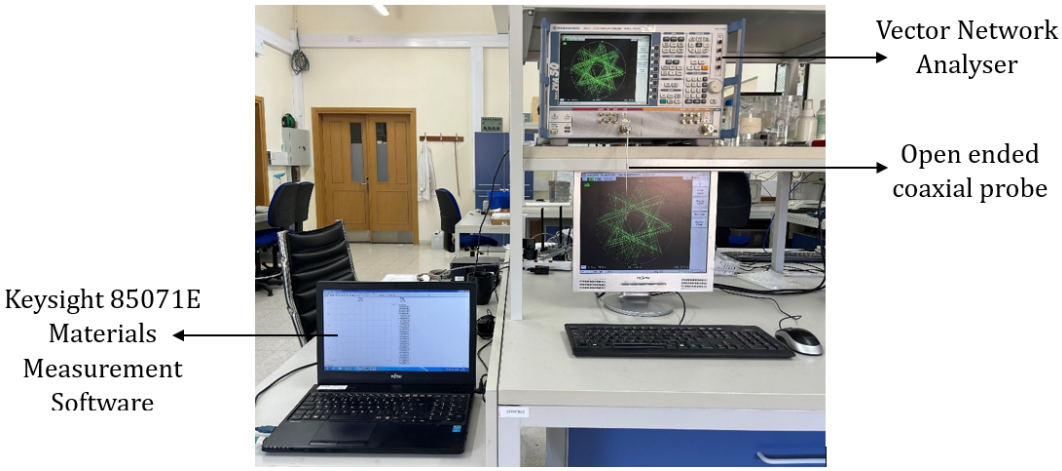

Figure 3.1: Setup of the VNA, probe and the software used

3.5.2 Calibration Procedure

Calibration was performed before each set of dielectric measurements to ensure accuracy when using an open-ended coaxial probe with the VNA. The calibration process consisted of two main stages: calibration at the port (connector) plane and at the probe's open end, ensuring precise measurements of dielectric properties.

Initially, the VNA was calibrated at the port plane using a standard set of loads: open, short, and matched. This step established a reference for the reflection coefficient measurements to the probe aperture plane. Direct calibration was performed at the tip of the open end of the probe, following a three-step procedure. This involved calibrating with the probe exposed to air (open) (Figure 3.2a), then shorting the probe using a shorting block to achieve full reflection (Figure 3.2b), and then immersing the probe tip in deionised water (Figure 3.2c). Deionised water was chosen for its well-known dielectric properties, low cost, and nontoxicity, making it an ideal calibration standard. The calibration was performed in a set frequency range between 500 MHz and 50 GHz, with 201 data points

to ensure a high-resolution measurement. The validity of the calibration procedure was confirmed by measuring the permittivity of a 0.1 mol/L NaCl solution at room temperature, a standard with well-documented dielectric properties. This consistent and rigorous calibration process, conducted before each data collection session, minimised uncertainties and ensured the reliability of the dielectric property measurements obtained during this study.

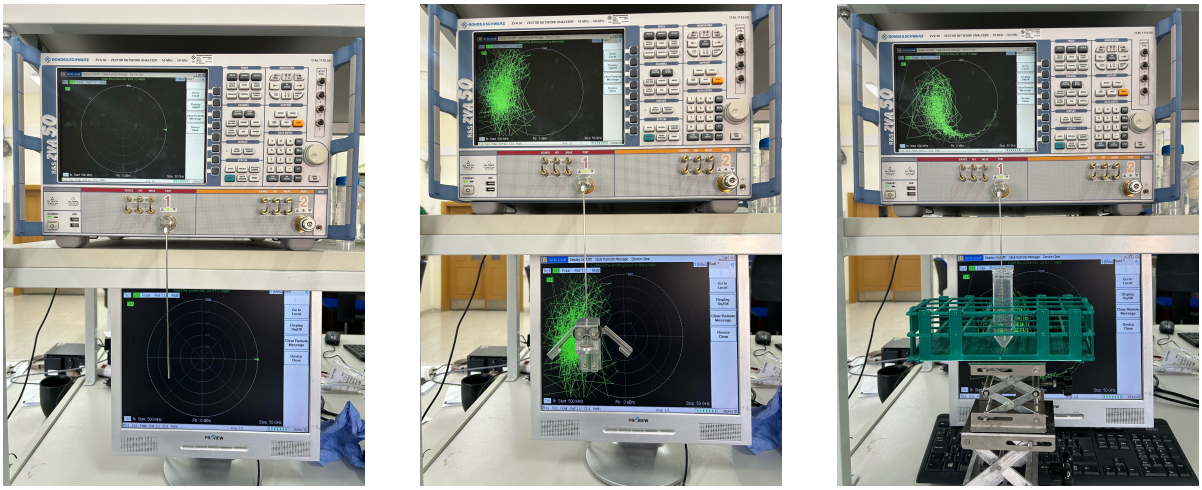

(a) Exposed to air (b) Shorting block (c) Immersed in water

Figure 3.2: Three-step calibration procedure

3.5.3 Phase 1: Familiarisation with Complex Permittivity Measurement Technique

Before fabricating the phantoms needed for this study, it was essential to familiarise with the measurement of complex permittivity by using standard liquids, namely ethanol and 0.1 mol/L NaCl. These liquids were chosen due to the availability of well-established dielectric models in the literature and their ease of access This phase involved practical experience with the VNA, specifically the Rhode and Schwarz ZVA-50 and the open-ended coaxial probe. After calibration, the probe was immersed in standard liquids. It was important to ensure good contact between the probe and the liquid, making sure there were no air bubbles that could affect the accuracy of the measurements. Using the probe, the

S11 parameters were obtained for the standard liquids. Multiple readings were taken to ensure accurate readings were obtained. The Keysight 85071E Materials Measurement Software was then used to convert these S11 parameters into complex permittivity values. This conversion process is based on well-established methodologies, including those detailed in papers by Stuchly and Stuchly (1980) and Marsland and Evans (1987). This software allows for the plotting of relative permittivity as a function of frequency, providing a visual representation of how the material's permittivity changes across the measured frequency range.

3.5.4 Phase 2: Dielectric Measurements of Fat, Skin and Tumour Mimics for Phantoms

In this phase, the fabrication of phantom mimics for skin, fat, and tumours was carried out to ensure accurate replication of their dielectric properties. The methodologies were primarily guided by the protocols detailed by Boparai and Popovic (2022), with additional insights drawn from the foundational work by Lazebnik et al. (2005). The aim was to accurately replicate the dielectric properties specific to these tissues, ensuring that the phantoms could be used in microwave diagnostic applications. The separate fabrication of these mimics was crucial for later combining them into comprehensive oil-in-gelatin phantoms. The ingredients used can be seen in Figure 3.3.

Figure 3.3: Ingredients used in the fabrication of the oil-in gelatin phantoms. From left to right: Kerosene oil, 200 Bloom Gelatin, deionised water (two separate bottles), p-toluic acid, sunflower oil (back), safflower oils (front), Propan-1-ol.

- **Fabrication of Skin Mimic:**

  The fabrication of the skin mimic started by dissolving 0.294 g of p-toluic acid in 28.69 ml of n-propanol. This was followed by mixing with 279.5 ml of deionised water. The mixture was then heated with 50.02 g of 200 Bloom gelatin at 90 °C, under constant stirring, until a clear solution was obtained. This gelatin mixture was then cooled to 50 °C in a water bath.

  In parallel, an oil mixture consisting of 98.6 ml of sunflower oil and kerosene, in equal proportions, was prepared and heated to 50 °C. The oil and gelatin solutions were then combined, with 5.86 ml of detergent added to stabilise the emulsion. The mixture was thoroughly stirred and poured into plastic tubes (as seen in Figure 3.4b), where it cooled and solidified, forming a skin mimic.

- **Fabrication of Tumour Mimic:**

  For the tumour mimic, 0.346 g of p-toluic acid was dissolved in 17.0 ml of n-propanol. The solution was then mixed with 328.0 ml of deionised water. The mixture was heated with 58.67 g of 300 Bloom gelatin at 90 °C, ensuring that the gelatin was fully dissolved to form a transparent solution. After cooling to 50 °C, 38.4 ml of oil mixture (sunflower and kerosene, 50:50) was prepared and heated. The gelatin solution was emulsified with the oil mixture, with 2.0 ml of detergent added to stabilise the emulsion. The mixture was then poured into plastic tubes (as seen in Figure 3.4b) and allowed to solidify, forming the tumour mimic.

- **Fabrication of Fat Mimic:**

  The fabrication of the fat mimic presented unique challenges due to the high oil content required to simulate the low permittivity of human fat tissue. The standard procedure began with dissolving 0.133 g of p-toluic acid in 6.96 ml of n-propanol,

followed by mixing this solution with 132.7 ml of deionised water. Next, 24.32 g of 200 Bloom gelatin was added and heated to 90°C until fully dissolved, resulting in a transparent solution. However, the large volume of oil (265.6 ml of a 50:50 sunflower oil and kerosene mixture) posed a difficulty in maintaining a stable emulsion within the gelatin matrix (as seen in Figure 3.4a).

A modified method was used to address the issue of phase separation. Instead of adding the entire oil mixture at once, the gelatin solution was kept under continuous stirring and gentle heating using a magnetic stirrer/heater. The oil was then gradually introduced using a pipette, allowing for controlled addition and better integration into the gelatin mixture. This incremental approach, combined with the continuous stirring, helped to stabilise the emulsion and prevented the oil from separating. Moreover, 12.0 ml of detergent was carefully added during the stirring process to further stabilise the emulsion and ensure uniform dispersion of oil droplets.

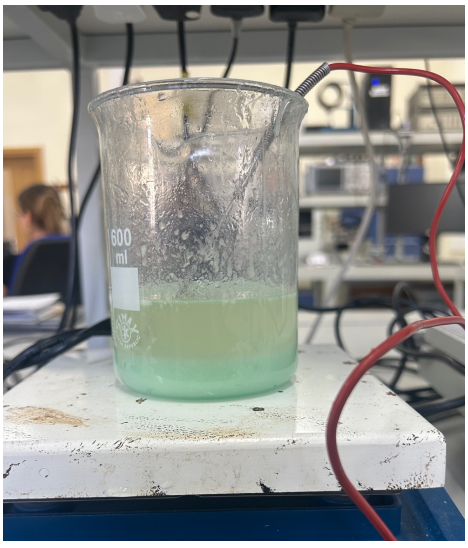

(a) Initial problem when fabricating the Fat Mimic

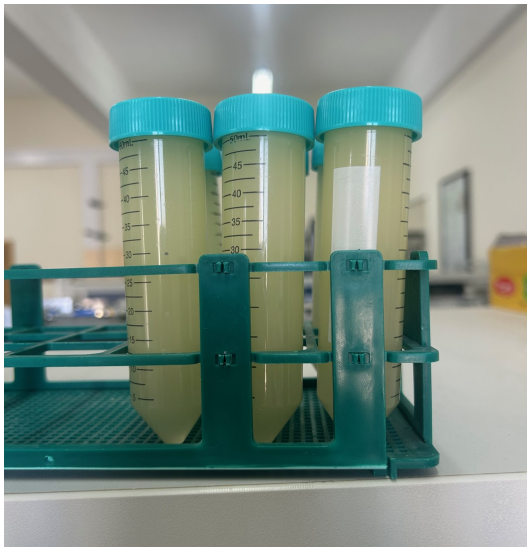

(b) Final mixture poured into plastic tubes to solidify

Figure 3.4: Photos taken during mimic fabrication

After allowing each mimic to solidify overnight, its dielectric properties were measured the following day over a frequency range of 500 MHz to 50 GHz using the VNA and the open-ended coaxial probe. The probe was immersed into the mimics to achieve stable and consistent contact between the probe and the sample. This was possible because of the gel-like consistency of the mimics, which facilitated immersion. All measurements were performed at room temperature (23 °C). The measurements of each mimic were taken at different depths and averaged. After each measurement, the probe was properly cleaned with ethanol and deionised water to prevent oil accumulation on the probe's surface.

The reflection coefficients (S11) obtained from the VNA were converted to the real and imaginary parts of the complex permittivity using Keysight 85070E software. The shelf life of each mimic was analysed up to 24 weeks after fabrication. A reproducibility test was also performed for each mimic to assess the consistency of the measurements obtained. The results obtained from these measurements are presented in Section 4.2.1.

3.6 Research Methodology: Data Collection Tool

In this section, Phase 3 of the study is discussed, focusing on the fabrication of multilayer oil-in-gelatin phantoms, which served as data collection tools in this research to measure dielectric properties and evaluate the results obtained. This phase began after confirming that the dielectric properties of the mimics aligned with the existing literature during Phase 2 (as detailed in Section 4.2.1).

3.6.1 Outer casing of the oil-in-gelatin phantom:

The first step involved the fabrication of the outer casing of the phantom using 3D printing. The Ultimaker S5 printer was used, located in the Electromagnetism Lab at the University of Malta. The outer casing design was created using Fusion 360 by Autodesk and the 3D printing parameters were configured using Ultimaker Cura 5.8.0 software. The

design and dimensions of the outer case are illustrated in Figure 3.5.

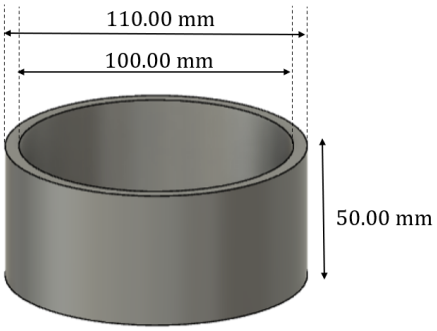

Figure 3.5: Outer casing design and dimensions created with Fusion 360 by Autodesk.

Since the mimics were poured into the case while still in liquid form at approximately 50 °C, it was important to ensure that the casing was both watertight and resistant to high temperatures. A pilot study was conducted to verify these requirements, as detailed in Section 3.8. The material selection and 3D printing parameters for the final case (Table 3.1) were based on the results of this pilot study.

Print and Filament Settings	**Parameter**
Filament Type	PETG
Layer height (mm)	0.1
First layer height (mm)	0.1
Wall Line Count	5
Wall Thickness (mm)	1.2
Bottom Horizontal Solid Layers	12
Bottom Thickness (mm)	1.2
Seam Position	Sharpest Corner
Infill Density (%)	60
Infill Pattern	Grid
Nozzle Temperature (°C)	240
Bed Temperature (°C)	80
Generate Support Material	Enabled

Table 3.1: Parameters for 3D printing the outer case.

3.6.2 Fabrication of the Oil-in-gelatin Phantoms:

1. **Step 1: Fabrication of the Fat mimic**

   Once the outer casing was printed, the fat mimic was fabricated and poured into the casing, following the steps detailed in Section 3.5.4. The fat was poured to a thickness of 8 mm within the case. After the fat mimic was poured into the phantom, its dielectric properties were measured the next day and validated against the reference values obtained when the mimic was initially prepared during Phase 2, before proceeding with the next layer.

(a) Gelatin mixture at 90°C under constant stirring.

(b) Oil mixture introduced in the gelatin mixture

(c) Fat poured into the phantom's case.

Figure 3.6: Fat mimic

2. **Step 2: Fabrication of Coin-shaped Hollow for Tumour Mimic Insertion**

   To accommodate the later insertion of the tumour mimic, a coin-shaped void was created at the top of the fat layer. To determine the most effective method for creating this void in the fat mimic, two different approaches were tested as part of a pilot study. The pilot study, detailed in Section 3.8.3, used a smaller scale model to minimise printing time and material consumption. The final approach was selected based on its ability to minimise human error and its ease of sealing in conjunction with the phantom casing, ensuring air tightness and contributing to the phantom's extended shelf-life of several weeks. The initial pilot design, as shown in Section

3.8.3, had a cuboidal base; however, this was later replaced by a cylindrical base that matched the dimensions of the phantom's outer casing. This modification provided greater stability and improved air tightness, functioning as a lid while the fat layer solidified.

The dimensions of the design allowed for the creation of a tumour void within the fat mimic, achieving a depth of 3 mm and a diameter of 20 mm. The height of the inner walls of the phantom case measured 40 mm, while the design itself was 35 mm in height. With the fat mimic set to a height of 8 mm, the insertion of the design on top of the case resulted in a precise 3 mm-deep hollow. This ensured that the tumour mimic could be accurately placed within the fat mimic, creating a clearly defined and consistent space for further dielectric property measurements.

Figure 3.7a represents the design for the coin-shaped hollow using Fusion 360, while Figure 3.7b presents the corresponding 3D printed result. A detailed schematic of the setup used for forming the coin-shaped void in the fat mimic is shown in Figure 3.8. The lab setup can be seen in Figure 3.9a. This setup was left undisturbed for 24 hours for the fat to solidify and the hole for the tumour insertion to form. Lastly, 3.9b presents the final outcome, highlighting the precise void created in the fat mimic.

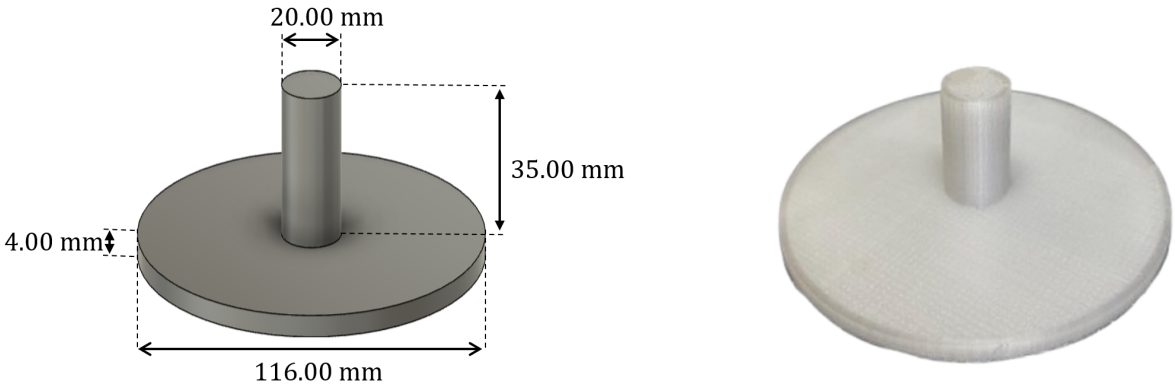

(a) Design on Fusion 360 (b) 3D Printed Result

Figure 3.7: Design of the coin-shaped hollow for the tumour insertion.

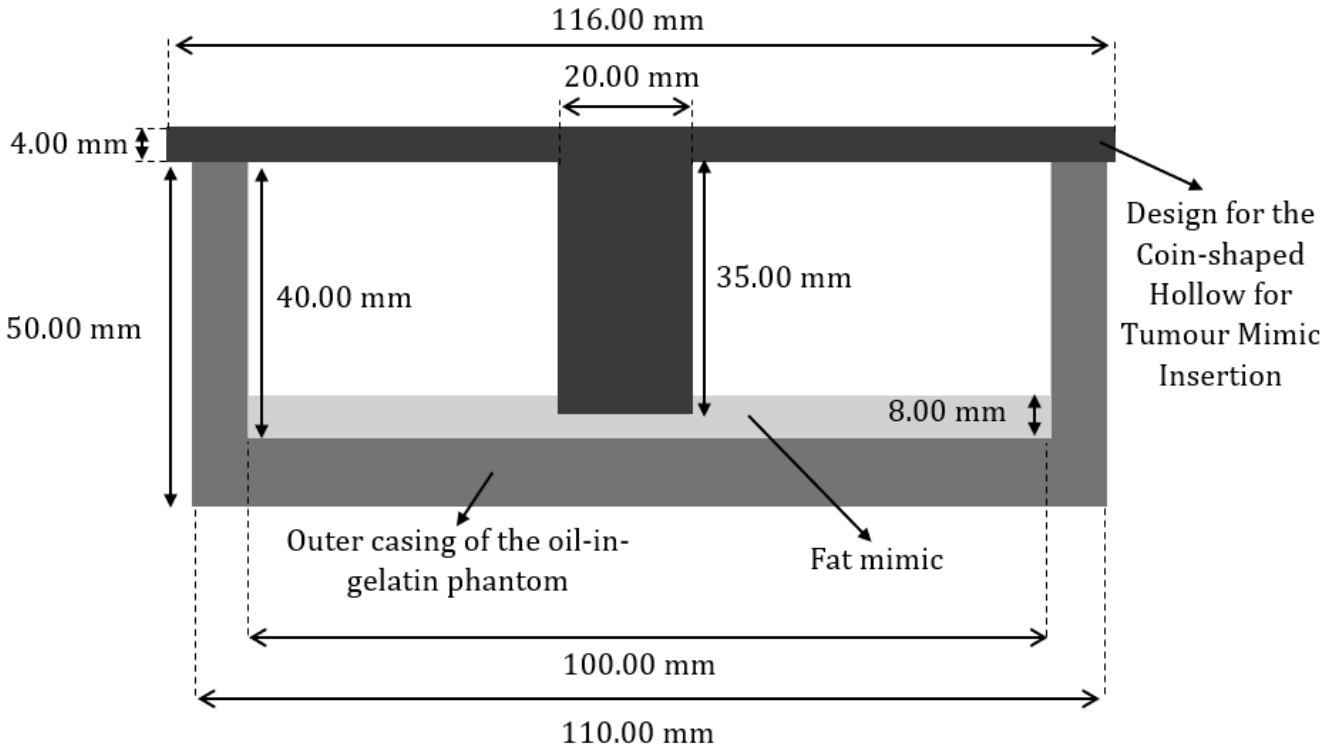

Figure 3.8: Schematic diagram for the creation of the coin-shaped hollow for tumour insertion.

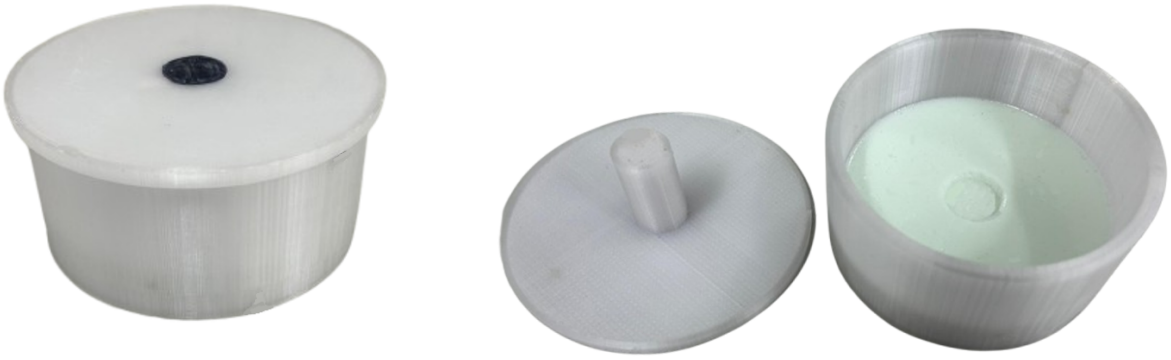

(a) Lab set up (b) Final result

Figure 3.9: Lab results for the creation of the coin-shaped hollow for tumour insertion.

3. **Step 3: Fabrication of the Tumour mimic**

   The tumour mimic was fabricated following the steps detailed in Section 3.5.4. Using a pipette, the mimic was carefully poured into the 3 mm depth hole in the fat mimic, as seen in Figure 3.10. The phantom was then left for 24 hours, allowing the tumour to solidify. Once solidified, its dielectric properties were measured to ensure that they matched the dielectric characteristics of the tumour tissue.

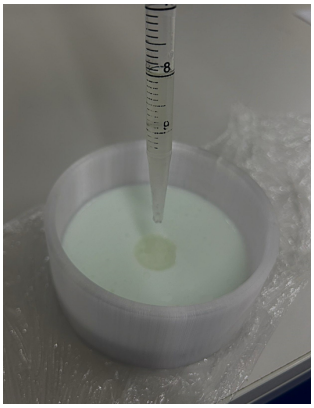

Figure 3.10: Tumour mimic poured in phantom.

4. **Step 4: Fabrication of the Skin mimic**

   The skin mimic was fabricated following the steps described in Section 3.5.4. The skin mimic was lowered using a pipette on top of the fat and tumour, forming a 2 mm thick layer. This thickness was selected based on the evaluation of the existing literature, particularly the study by Akkus et al. (2012), as it provided valuable insight into the appropriate thickness for mimicking human skin tissue.

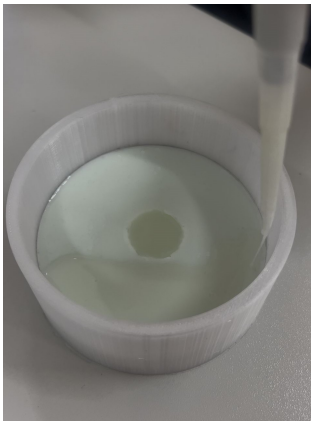

Figure 3.11: Skin mimic poured in phantom.

In addition to the fabricated phantom mentioned containing skin, fat, and tumour, a second identical phantom was fabricated without the skin layer. This additional phantom allowed for an evaluation of the effect of the skin in the detection of tumours, specifically liposarcoma, using microwave techniques. The dielectric properties of human skin and tumour tissue are relatively similar, which can challenge the detection of tumours underneath the skin. By comparing the results of both phantoms, one having a 2 mm thick skin layer and the other without, this study aimed to evaluate the influence of skin on microwave tumour detection.

Furthermore, during the preparation of the oil-in gelatin phantom containing the fat, tumour, and skin mixtures, as described above, small portions of these individual mixtures were also poured into separate plastic tubes for testing. These samples were analysed to measure their dielectric properties the day after fabrication to make sure that they agree with the previous mimics fabricated during Phase 2 as well as with the existing literature. The results of Phase 2, along with comparisons with values reported in the literature, are detailed in the Results section. The dielectric measurements obtained were in good agreement with previous results, confirming the accuracy and reliability of the phantom's dielectric properties. The dielectric properties of the mimics found in both phantoms can be seen in Figure 3.12.

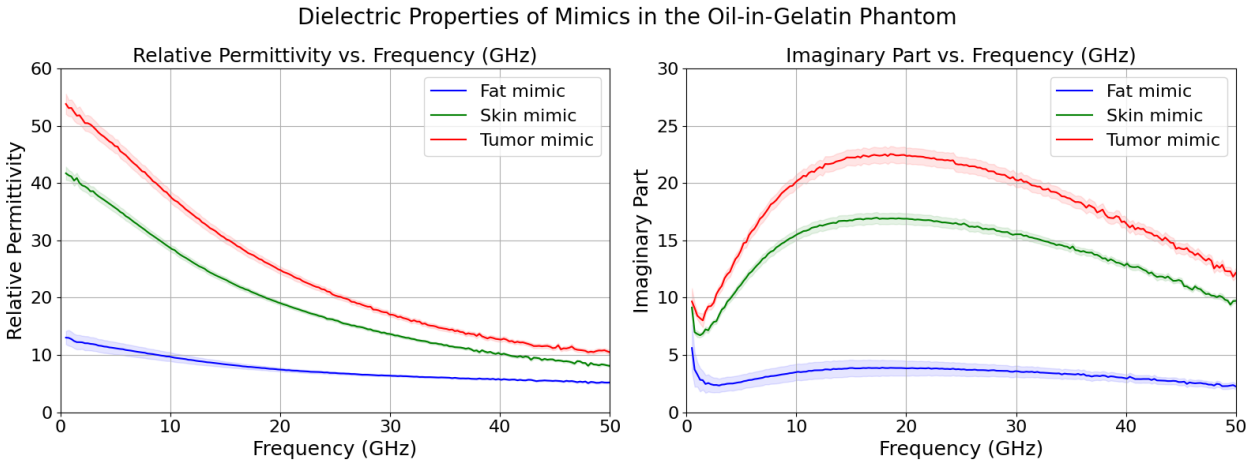

Figure 3.12: Dielectric properties of mimics in the oil-in gelatin phantoms

3.6.3 Selection of Measurement for Dielectric Properties of the Fabricated Phantoms:

Once the phantoms were fabricated, their dielectric properties at the surface were measured using the probe and VNA. With the help of Keysight 85070E software, the S11 parameters were converted to complex permittivity, providing real and imaginary parts. Before any measurements were taken, the VNA was calibrated to ensure the accuracy and reliability of the results.

A 3D printed grid as seen in Figure 3.13a was used and placed on top of the phantoms when taking measurements (Figure 3.13b). This grid featured square holes measuring 3 mm by 3 mm spaced 2 mm apart to ensure that the probe was inserted in equidistant locations across the phantom's surface. The small size of the holes minimised lateral movement when the probe was inserted. The use of this grid ensured that measurements could be reproduced reliably, with the probe inserted at the same points during each measurement session, maintaining consistency between multiple experiments. Each square hole in the grid was assigned a specific coordinate to help with visualisation of the dielectric properties, which will be discussed in the next section (Data Analysis). The grid contained a total of 400 square holes; however, not all holes were used for measurements, as the phantom itself was circular. Furthermore, the probe was always inserted at the same depth, making sure that measurements were taken at the same level on the phantom's surface.

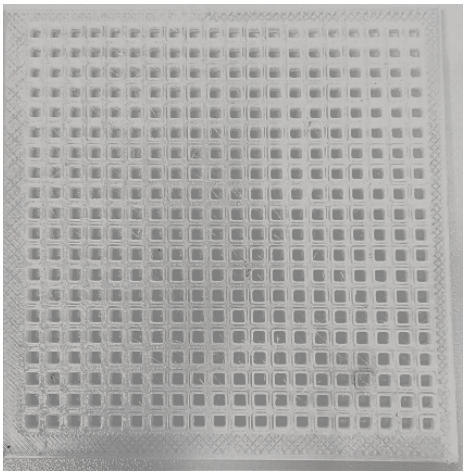

(a) 3D printed grid

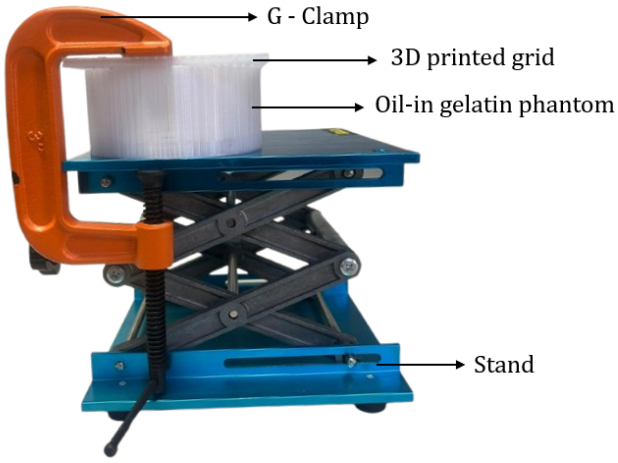

(b) Lab setup

Figure 3.13: 3D printed grid used for dielectric property measurements and its setup

To ensure stability throughout the procedure, a G-clamp was used to secure the phantom and the grid together, as seen in Figure 3.13b. Additionally, double-sided tape was ap-

plied to further minimise any movements, ensuring that the phantom remained fixed and unintended shifts did not influence the results during measurements.

3.7 Data Analysis Technique

One of the objectives of this study was to visualise the microwave reflectometry data to assess its ability to detect liposarcoma. As discussed above, two phantoms, one with skin and one without, were used to examine and compare the skin's effect on producing images based on dielectric spectroscopy. Phase 4 will be discussed in this section.

In order to obtain spatial information on the dielectric properties of the phantom's surface, specific coordinates were assigned to the square holes in the 3D printed grid, the bottom left square being the origin. These coordinates corresponded to the locations where dielectric measurements were taken. The grid ensured that the probe was consistently positioned at known, equidistant points across the phantom, enabling spatially organised data collection. The probe remained stationary throughout the measurement procedure, and only the phantom was moved to each measurement point. The probe was inserted to 34 mm for the phantom with skin and 36mm for the one without. To maintain consistency, the probe was marked to ensure that the same depth was used for all measurements in a phantom. The probe was also carefully cleaned between measurements, particularly around tumour boundaries. The insertion depths for each phantom can be seen in Figure 3.14.

Each measurement location followed a structured procedure in which the S11 parameters were recorded using the VNA, and these parameters were converted to complex permittivity using Keysight software. The readings were taken at multiple locations on the phantom's surface to build a comprehensive dielectric profile. At each location, multiple readings were taken and averaged to improve accuracy. Using precise coordinates for each

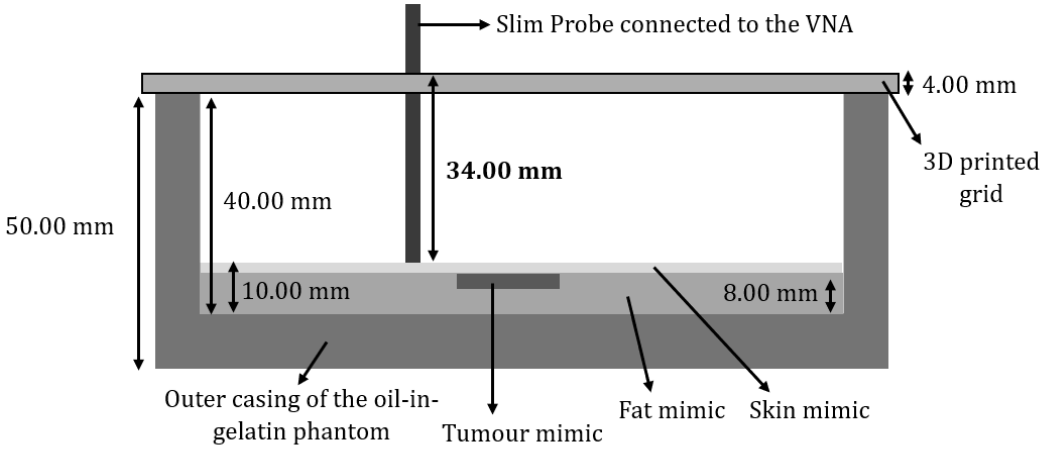

(a) Depth of the probe - Phantom with skin mimic

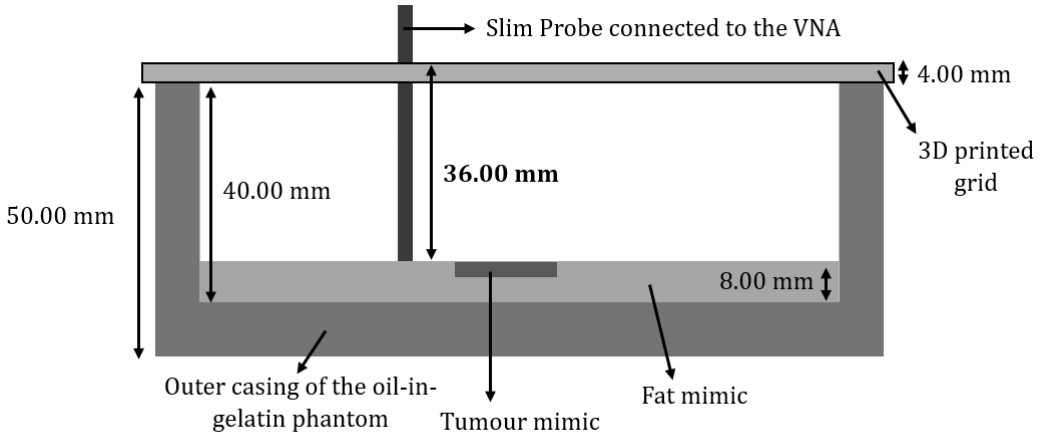

(b) Depth of the probe - Phantom without skin mimic

Figure 3.14: Depth of probe in phantoms during measurements

measurement, the dielectric properties (real and imaginary permittivity) were mapped and visualised as permittivity maps, the x- and y-axes representing spatial locations, and the colour intensity indicating the dielectric values. This analysis was performed with Python. Permittivity maps were chosen for their ability to observe the contrast in dielectric properties between tumour and non-tumour regions. The constant power level was set to 0 dBm and all measurements were taken at room temperature (24 °C).

3.8 Pilot Study

3.8.1 Sunflower vs. Safflower oil for the Mimics

A preliminary pilot study was conducted to determine the oil most suitable for use in the fabrication of tumour mimics, based on their dielectric properties. This pilot study aimed to compare the dielectric properties of phantoms made using two different oil combinations: safflower oil and kerosene, versus sunflower oil and kerosene. The comparison was essential to identify an oil mixture that closely aligns with the dielectric properties reported in existing literature, particularly the study by A. Martellosio et al. (2016) and Lazebnik et al. (2007).

To minimise the consumption of materials during this preliminary phase, each phantom mimic was prepared using 50% of the required materials specified in the fabrication protocol [Boparai and Popović, 2022b]. This approach allowed for evaluation without excessive use of resources. The tumour mimics were tested using the open-ended coaxial probe and the results were plotted against the reference data from the literature. Figure 3.15 presents a comparison of the relative permittivity and the imaginary part (loss factor) as functions of frequency, ranging up to 50 GHz.

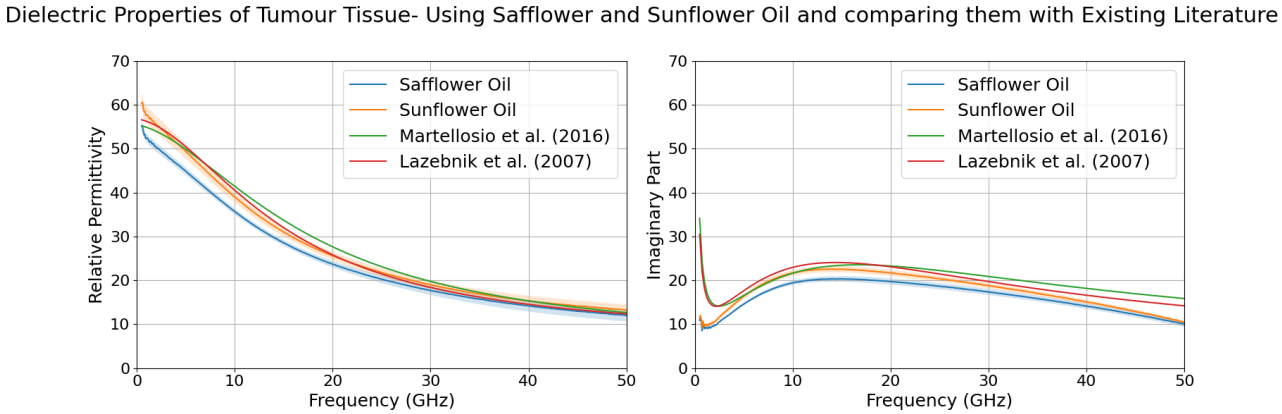

Figure 3.15: Comparing lab results of tumour mimics (with Safflower oil and Kerosene, and Sunflower oil and Kerosene) with existing literature

The mimics prepared with sunflower oil and kerosene demonstrated dielectric properties closer to the reference data from the existing literature, particularly in the higher frequency range, while the safflower oil and kerosene mixture showed a greater deviation.

Based on these findings, it was concluded that the sunflower oil and kerosene mixture was more suitable for phantom fabrication. This decision was further supported by practical considerations, as sunflower oil is more readily available and more cost-effective. For the final fabrication of mimics, sunflower oil was used in combination with kerosene.

3.8.2 Outer casing for the oil-in-gelatin phantom

Prior to printing the final outer casing, a smaller-scale prototype was designed using Fusion 360 by Autodesk and printed. This was done to verify the suitability of the 3D printing parameters to achieve water tightness and ensure that the selected material could withstand exposure to liquids at 50 °C. The prototype design and the 3D printed result are shown in Figure 3.16a and 3.16b respectively.

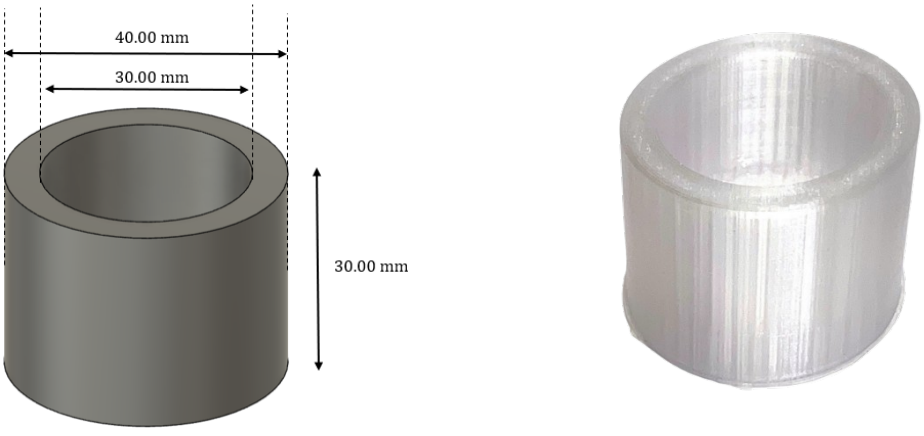

(a) Prototype design (b) 3D printed result

Figure 3.16: Outer casing of oil-in gelatin phantom - Prototype

The printing parameters used are described in Table 3.2.

Print and Filament Settings	**Parameter**
Filament Type	PETG
Layer height (mm)	0.1
First layer height (mm)	0.2
Wall Line Count	5
Wall Thickness (mm)	1.2
Bottom Horizontal Solid Layers	12
Bottom Thickness (mm)	1.2
Seam Position	Sharpest Corner
Infill Density (%)	40
Infill Pattern	Grid
Nozzle Temperature (°C)	240
Bed Temperature (°C)	80
Generate Support Material	Enabled

Table 3.2: Parameters for 3D printing the outer casing prototype.

The prototype casing proved to be both watertight and resistant to high temperatures, confirming the effectiveness of the selected 3D printing parameters and material. Based on the outcomes of this pilot study, the final outer casing for the oil-in-gelatin phantom was fabricated using the same design and printing specifications. However, to further ensure water tightness, the infill density was increased from 40% in the prototype to 60% in the final casing. This adjustment resulted in a slightly longer printing time but provided better assurance of the casing's integrity.

3.8.3 Fabrication of Coin-shaped Hollow for Tumour Mimic Insertion

First Approach:

A 10 mm diameter prototype was fabricated to create the insertion point for the tumour mimic within the fat mimic. This prototype consisted of a cylindrical shape with a diameter of 10 mm and a height of 3 mm. Attached to the cylinder was a 4 cm tall cylindrical handle, designed to help with placement. After the fat mimic was poured into the pro-

totype outer casing (Figure 3.16b), this 10 mm prototype was carefully inserted into the fat to create the designated space for the tumour mimic. This set-up was secured with a clamp, as shown in Figure 3.17c, and the fat mimic was left to solidify for 24 hours. After 24 hours, the prototype was removed, leaving behind a coin-shaped hollow at the top of the fat mimic (Figure 3.17d), ready for subsequent insertion of the tumour mimic.

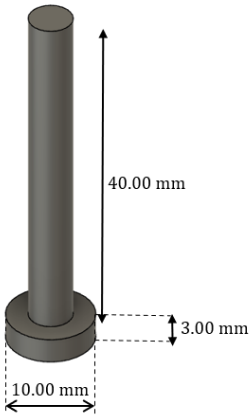

(a) Design on Fusion 360

(b) 3D printed result

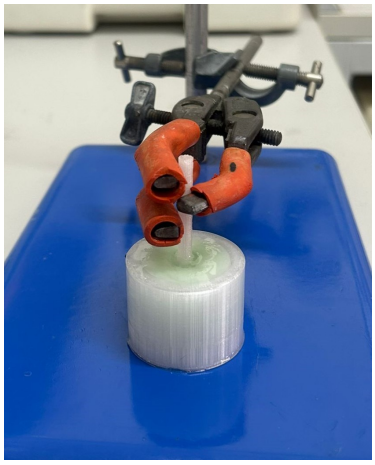

(c) Set up for the coin-shaped hollow

(d) Final result

Figure 3.17: Coin-shaped hollow on the top of fat mimic for tumour mimic insertion - First approach

Second Approach:

A prototype was designed and fabricated to create a precise insertion point for the tumour mimic within the fat mimic. The design featured a cylindrical section with a diameter of 10 mm and a height of 15 mm, which was attached to a cuboid base measuring 40 mm by 12 mm by 4 mm (Figure 3.18a). The height of the cylinder was set to 15 mm, corresponding to the inner depth of the phantom case where the fat mimic was placed, which was 20 mm. The primary focus of this pilot study was to test the feasibility of this approach for creating a coin-shaped hollow on top of the fat mimic.

As illustrated in Figure 3.18b, the prototype was inserted upside down into the fat mimic. The cuboid base provided stability and ease of manipulation during the insertion process. The cylindrical section of the prototype created a coin-shaped void within the fat. This setup was left undisturbed for 24 hours, allowing the fat mimic to solidify completely. Once solidified, the prototype was carefully removed, leaving behind a well-defined void in the fat mimic that would serve as the receptacle for the tumour mimic, as seen in Figure 3.18c.

(a) Design on Fusion 360 (b) Lab set up (c) Final result

Figure 3.18: Coin-shaped hollow on the top of fat mimic for tumour mimic insertion - Second approach

3.8.4 Grid for Dielectric Property Measurements

Before proceeding with the final grid design intended for the dielectric measurements of the fabricated phantoms, a pilot study was conducted. The primary focus of this study was to determine the ideal size of the square holes in the grid to allow the probe to pass through with minimal movement, thereby improving measurement accuracy.

Using Fusion 360, an initial design was created featuring two rows of square holes; one row with 3 mm holes, and a second row with 2.5 mm holes. This study showed that the 2.5 mm holes posed difficulty in inserting the probe, while the 3 mm holes allowed for easy insertion without any unnecessary movement, ensuring more reliable results. Thus, the final grid was designed with 3 mm square holes.

The same 3D printing parameters used for the outer casing were used to print the grid, however, due to having small dimensions, the print speed was reduced from 55 mm/s to 30 mm/s and the initial print speed was further decreased to 9 mm/s, leading to an improved final print.

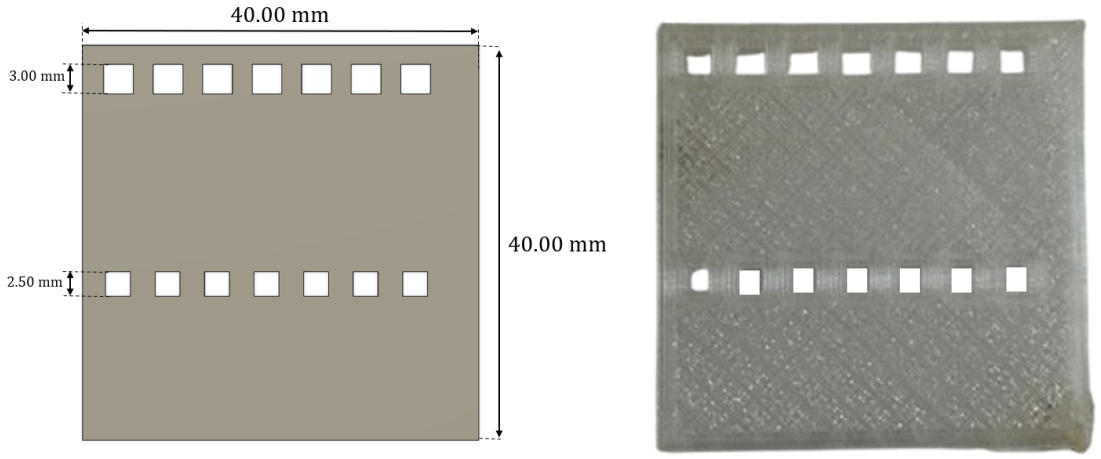

(a) Prototype design on Fusion 360 (b) 3D printed result

Figure 3.19: Pilot study for grid

3.9 Ethical Considerations

Permission to access and use the Electromagnetism Lab, including its specialised equipment such as the VNA and the Ultimaker 3D printer, was granted by Professor Lourdes Farrugia, Head of the Department of Physics at the University of Malta.

Furthermore, this study has been approved by the University Research Ethics Committee of the University of Malta.

3.10 Limitations of the Research Methodology

This study provided important insights into the dielectric properties of the oil-in-gelatin phantom and the detection of skin tumours using microwave technologies. However, several limitations must be recognised.

One key limitation was the restricted availability of existing literature on dielectric properties at frequencies up to 50 GHz. This made it difficult to compare the findings directly with other established studies.

The study was delimited mainly due to the performance of the probe and VNA used during this research. The open-ended coaxial probe method has emerged as a primary tool for measuring tissue dielectric properties. However, this method assumes that the sample is homogeneous and maintains good contact with the probe. Any factors such as air bubbles or uneven surfaces in the sample can lead to inaccuracies in measurements.

The dielectric measurements were sensitive to temperature fluctuations. Any minor variations in temperature during the experimental process could have influenced the results. The stability of the environment was maintained; however, the complete elimination of temperature effects was difficult.

Ensuring that the mimics were free of air bubbles was a challenge during the fabrication

process. Air bubbles could significantly alter the dielectric properties of the mimics, affecting the accuracy of the results.

Another constraint was the time available for phantom fabrication. Due to time limitations, it was not possible to produce multiple phantoms with varying skin thicknesses. This would have provided a more comprehensive evaluation of the effect of skin thickness on tumour detection using microwaves. Therefore, the study was limited to a single skin thickness of 2 mm, which may not fully capture the variability present in human tissue.

In addition, the casing of the oil-in gelatin phantom needed to be watertight. Although transparent PETG was used for 3D printing, the casing was not see-through, making it difficult to visually confirm the position of the probe when inserted. However, the probe was marked to ensure consistent insertion at the same depth during each measurement, maintaining accuracy despite limited visibility.

3.11 Conclusion

This chapter presented the research methodology used in the study. The next chapter will include the presentation and analysis of the results.

CHAPTER 4

Results

4.1 Introduction

This chapter presents the data, data analysis, and results obtained in this study.

4.2 Data

4.2.1 Phase 2: Dielectric Measurements of Fat, Skin, and Tumour Mimics

This subsection presents the dielectric properties of each mimic in comparison to existing literature. The results of the shelf life of each mimic are discussed, highlighting the stability of their dielectric characteristics over time. Furthermore, reproducibility tests are presented to evaluate the consistency and reliability of phantom preparation. This increased the robustness of this study.

Skin Mimic

The dielectric properties of the skin mimic were compared to the findings of Gabriel et al. (1996), who measured the dielectric properties of wet and dry skin. The laboratory results compared to the existing literature are shown in Figure 4.1a. Figure 4.1b presents the shelf life assessment of the skin after being poured into the plastic tubes. To ensure reproducibility of the mimic, a repeatability test was performed, with the results presented

in Figure 4.1c.

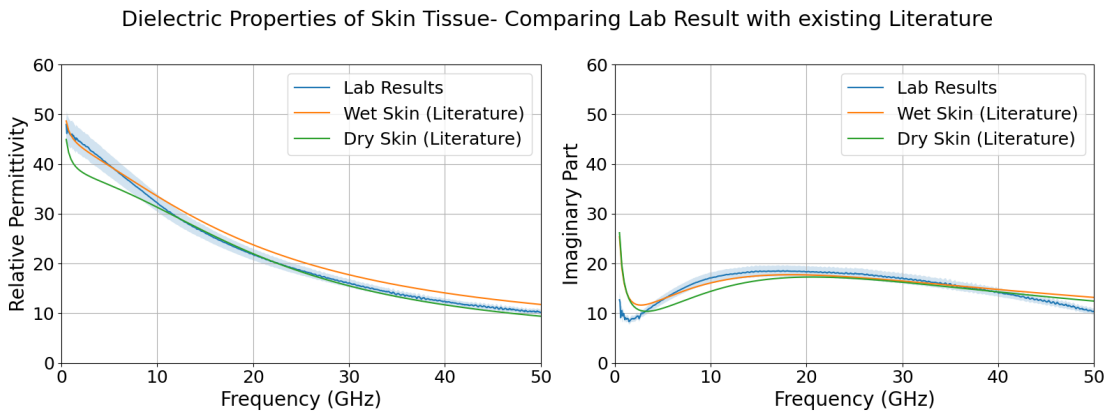

(a) Comparing lab results of skin mimic with existing literature - Gabriel et al. (1996).

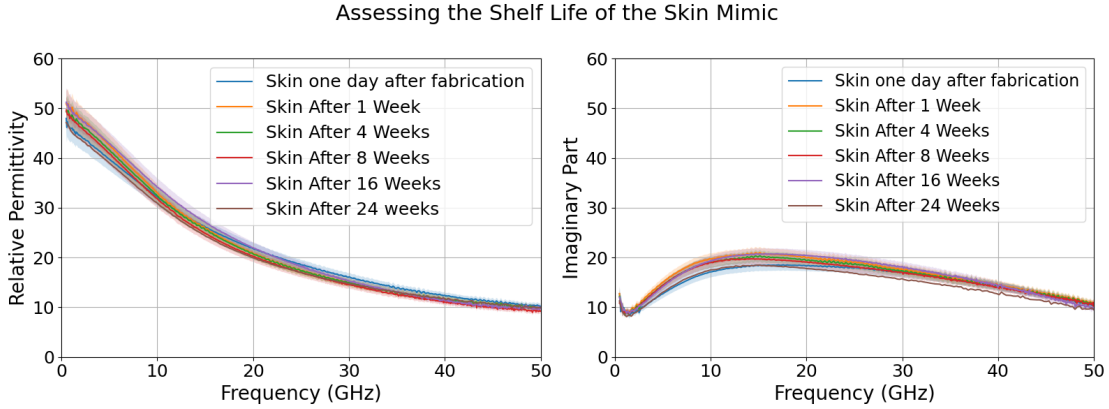

(b) Assessing shelf life of skin mimic.

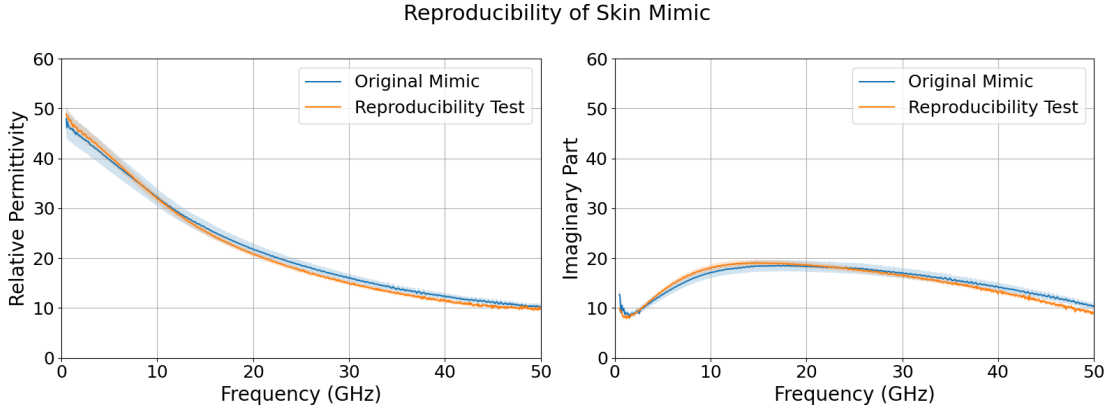

(c) Reproducibility test of skin mimic.

Figure 4.1: Comparison of laboratory results, shelf life, and reproducibility of skin mimic.

Tumour Mimic

The dielectric properties of the tumour mimic were compared with the findings of Lazebnik et al. (2007) and Martellosio et al. (2016). Lazebnik et al. (2007) evaluated the dielectric properties only up to a frequency of 20 GHz; thus beyond 20 GHz up to 50 GHz, extrapolations were made to compare with the data obtained in this study. Laboratory results in comparison to the existing literature are shown in Figure 4.2a. Figure 4.2b presents the shelf life assessment of the tumour mimic after it was poured into plastic tubes. In addition, a repeatability test was conducted, with the results presented in Figure 4.2c.

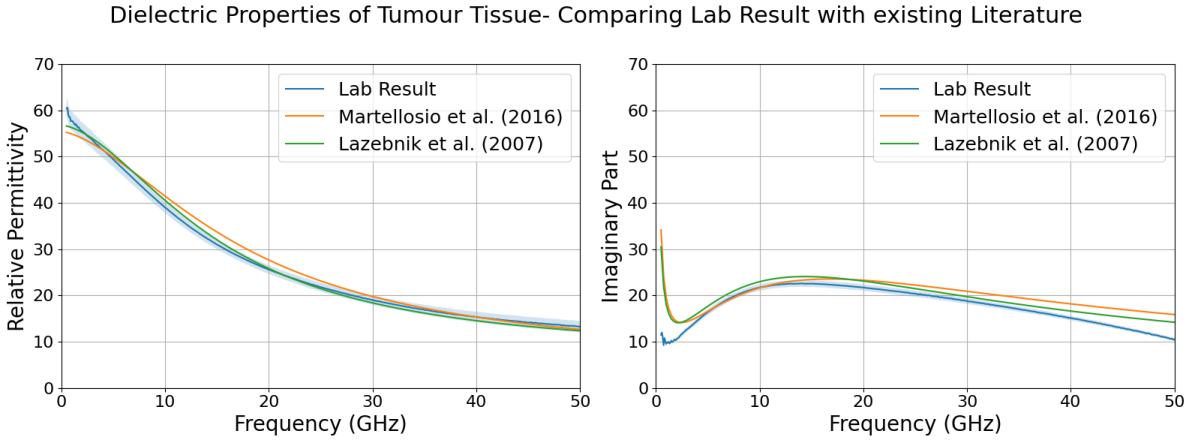

(a) Comparing lab results of tumour mimic with existing literature - Lazebnik et al. (2007) and Martellosio et al. (2016).

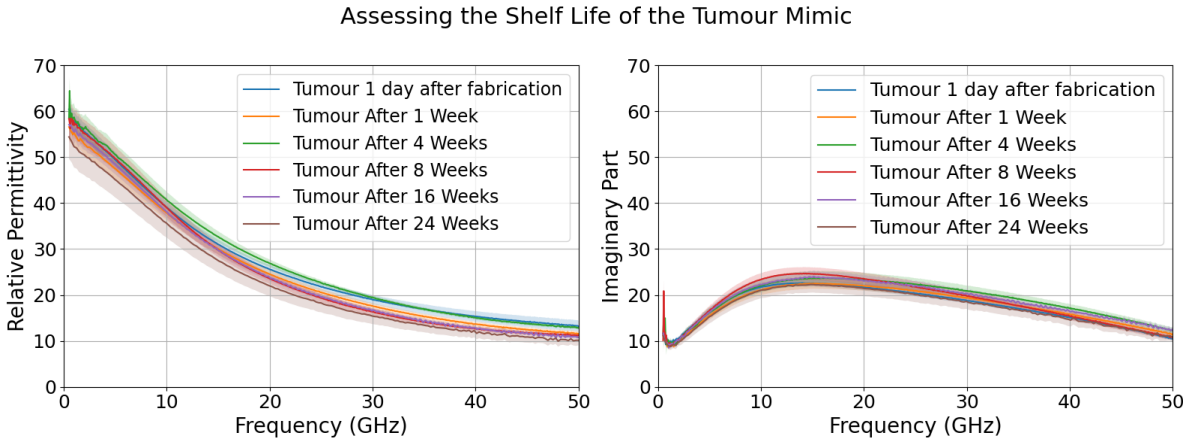

(b) Assessing shelf life of tumour mimic.

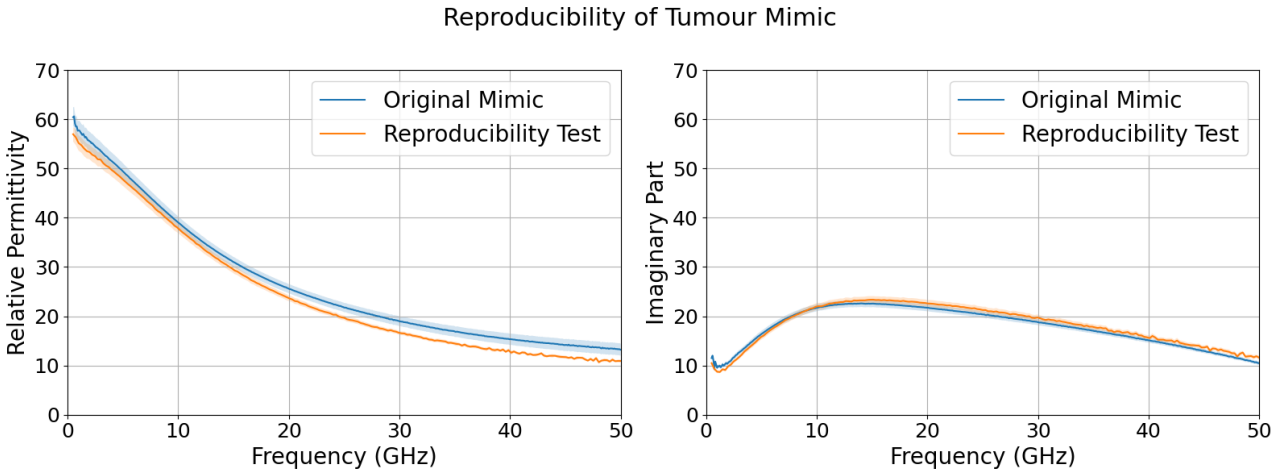

(c) Reproducibility test of tumour mimic.

Figure 4.2: Comparison of laboratory results, shelf life, and reproducibility of tumour mimic

Fat Mimic

The dielectric properties of the fat mimic were compared with the findings of Gabriel et al. (1996). Laboratory results in comparison to the literature are shown in Figure 4.3a. Figure 4.3b presents the shelf life assessment of the fat mimic after it was poured into plastic tubes. In addition, a repeatability test was conducted, with the results presented in Figure 4.3c.

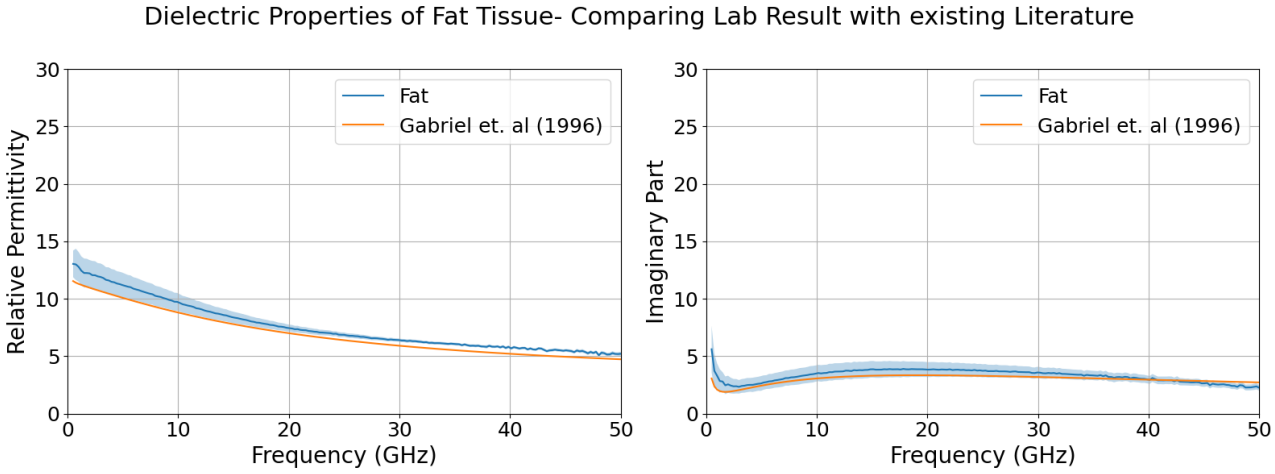

(a) Comparing lab results of fat mimic with existing literature - Gabriel et al. (1996).

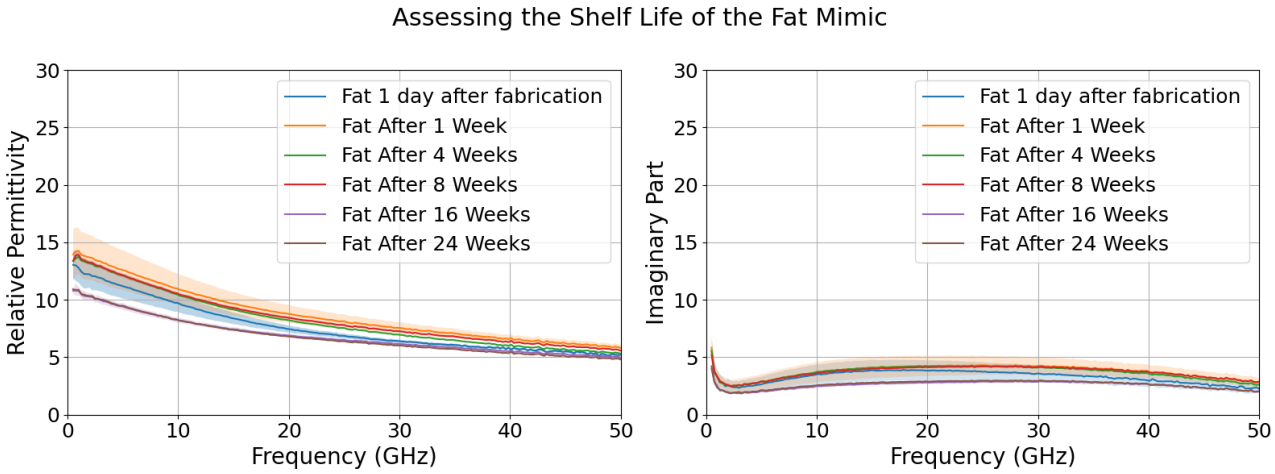

(b) Assessing shelf life of fat mimic.

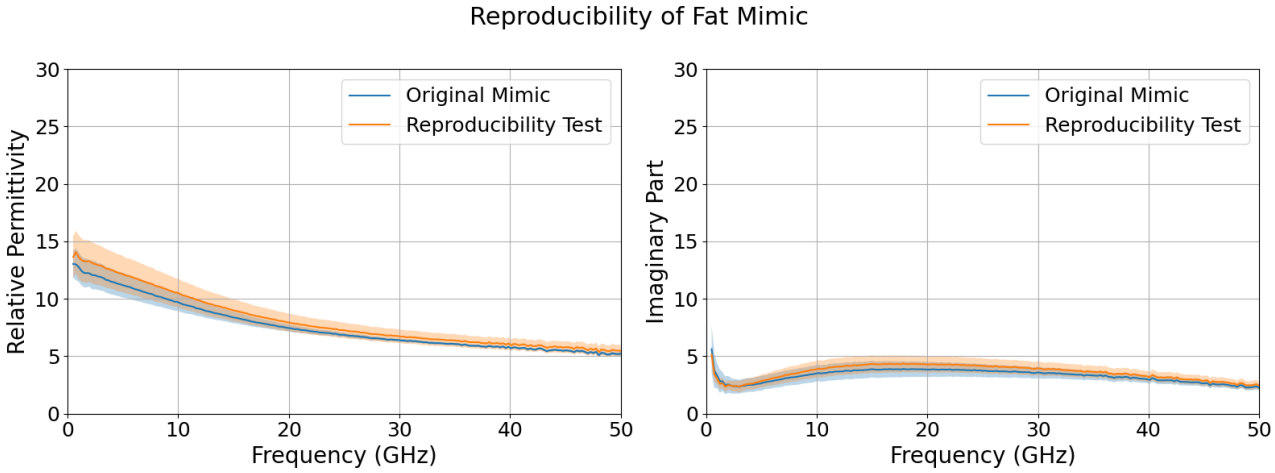

(c) Reproducibility test of fat mimic.

Figure 4.3: Comparison of laboratory results, shelf life, and reproducibility of fat Mimic.

4.2.2 Phase 3: Multilayer phantom fabrication and measurement of its dielectric properties

This subsection presents results related to the fabrication of the oil-in-gelatin phantoms, including the construction of the outer casing in which the phantoms were housed and the two different phantoms fabricated.

The oil-in gelatin phantoms - with and without skin

Figure 4.4: Oil-in-gelatin phantoms: from left to right—phantom with the skin mimic and phantom without the skin mimic

4.3 Data Analysis and Results

4.3.1 Phase 4: Dielectric maps for multi-layer phantom imaging

In this subsection, the results of the dielectric properties of the surface of both phantoms, with and without the skin mimic, are visualised and presented as permittivity maps.

The measurements were taken over a broad frequency range from 500 MHz to 50 GHz, but only particular frequencies were chosen for visualisation. A low, medium and high frequency of 900 MHz, 25 GHz and 50 GHz, respectively, were chosen. The frequency of 2.4 GHz was also included as it falls within the ISM band, which is widely used for electromagnetic medical devices. In Figures 4.5, 4.6, 4.7, and 4.8, presented in the following pages, the grey dots represent the individual measurement points where the probe recorded data on the phantom's surface. Using Python for data analysis, interpolation and extrapolation techniques were applied to transform these discrete measurements into continuous permittivity maps. The outer dashed circle presents the phantom's border, while the inner dashed circle indicates the location of the circular tumour within the phantom.

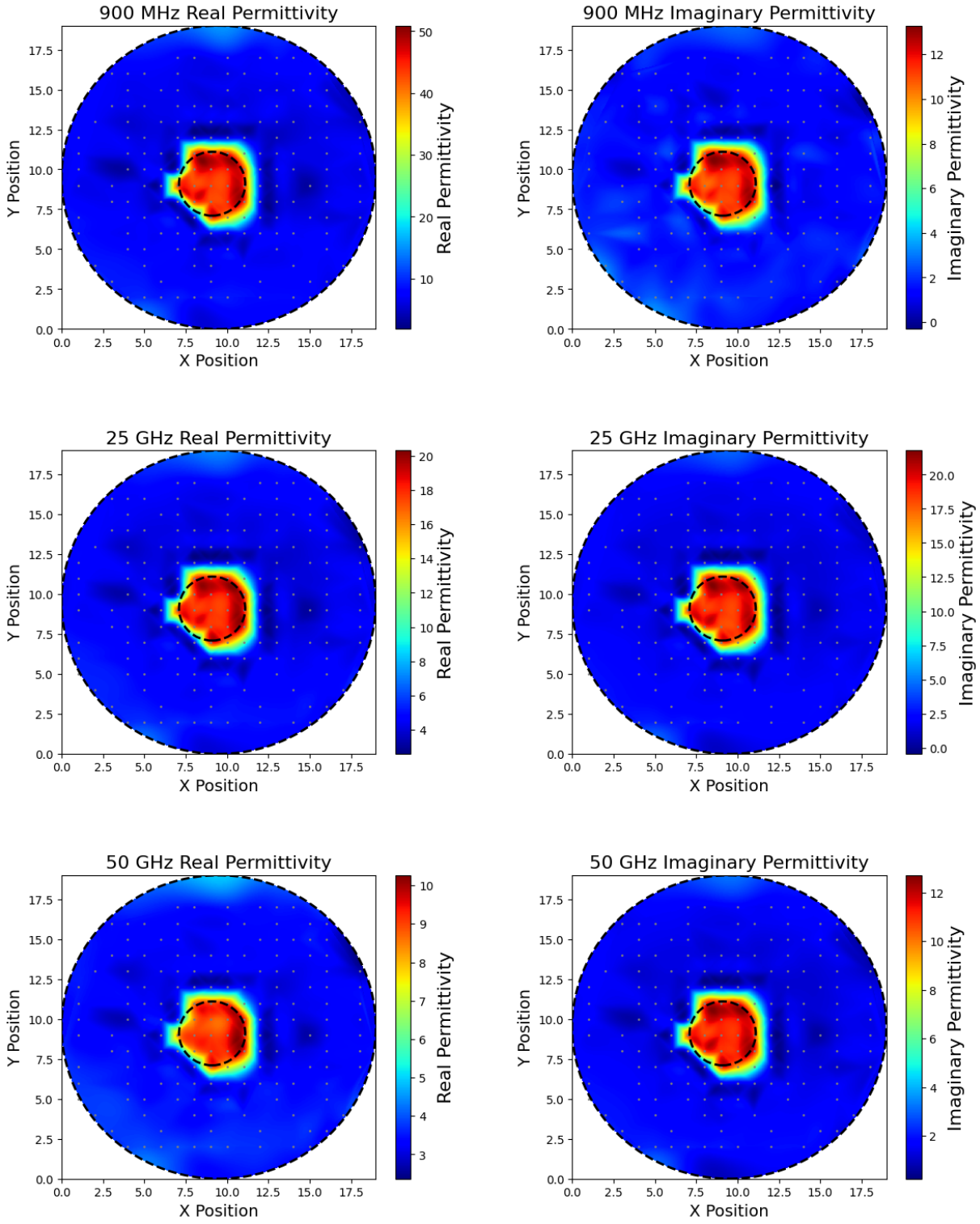

Figure 4.5: Dielectric properties at the surface of the oil-in gelatin phantom without skin mimic

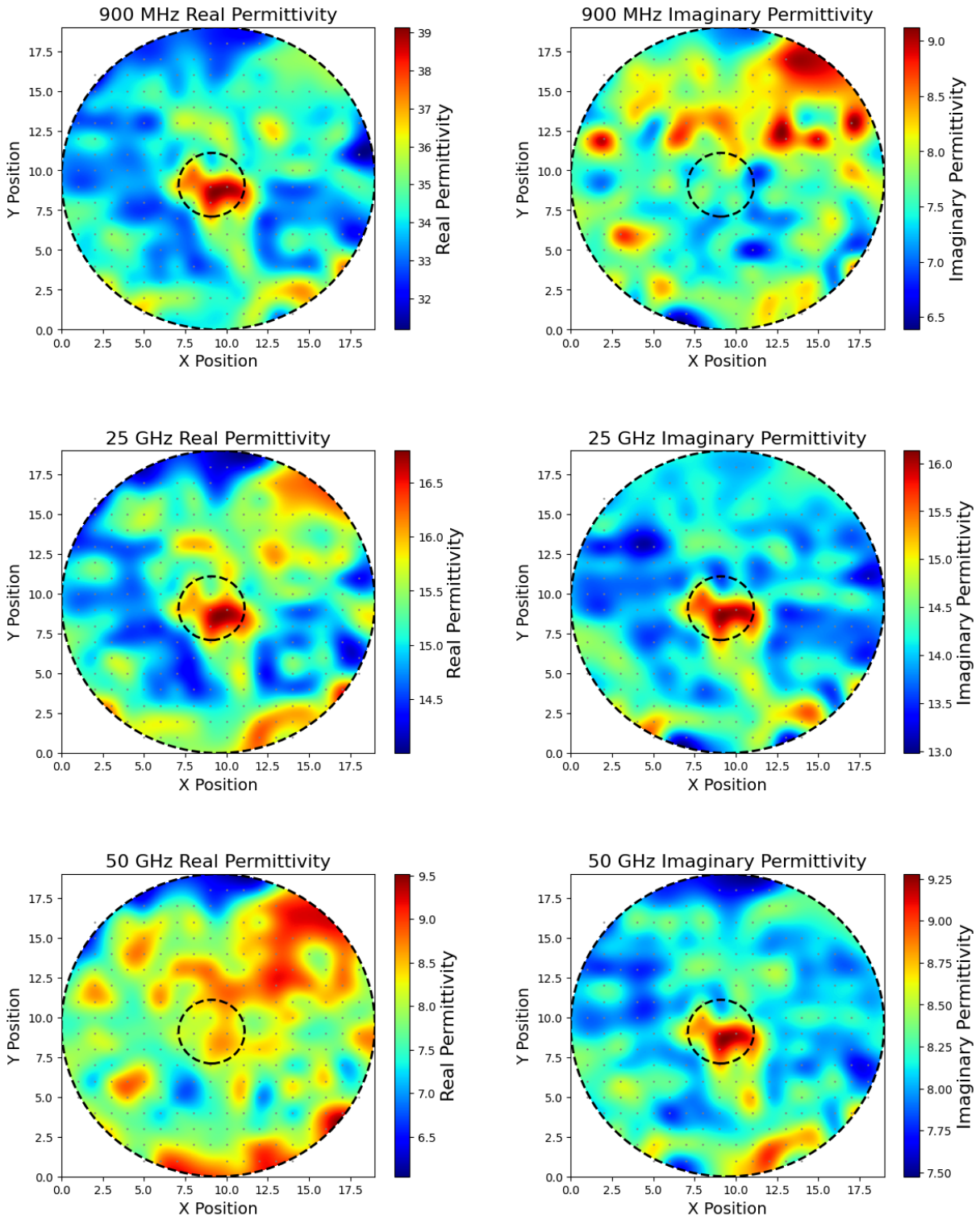

Figure 4.6: Dielectric properties at the surface of the oil-in gelatin phantom with skin mimic

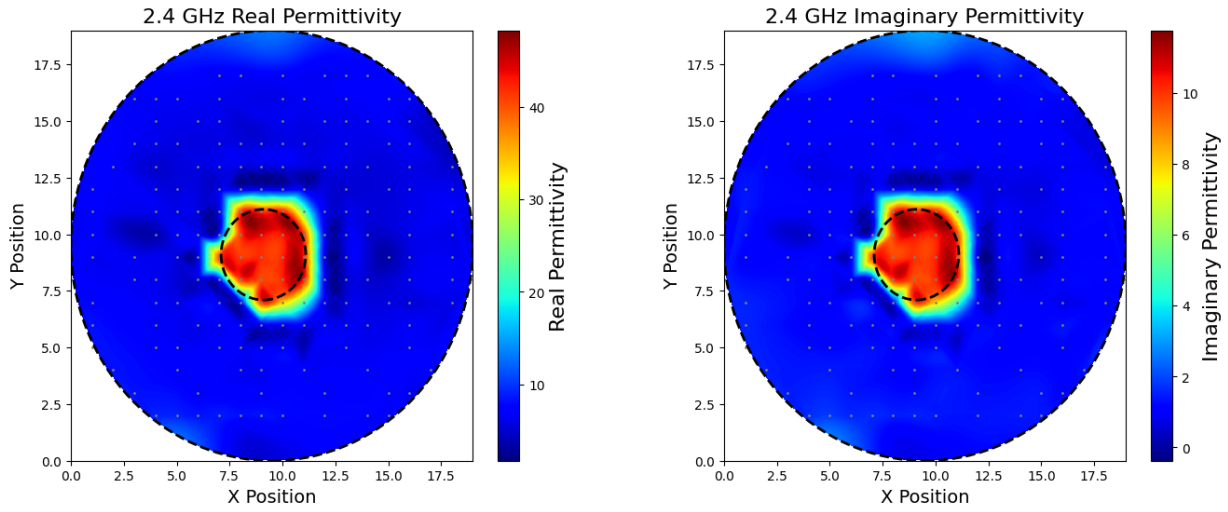

Figure 4.7: Dielectric properties at 2.4 GHz - Phantom without the skin mimic.

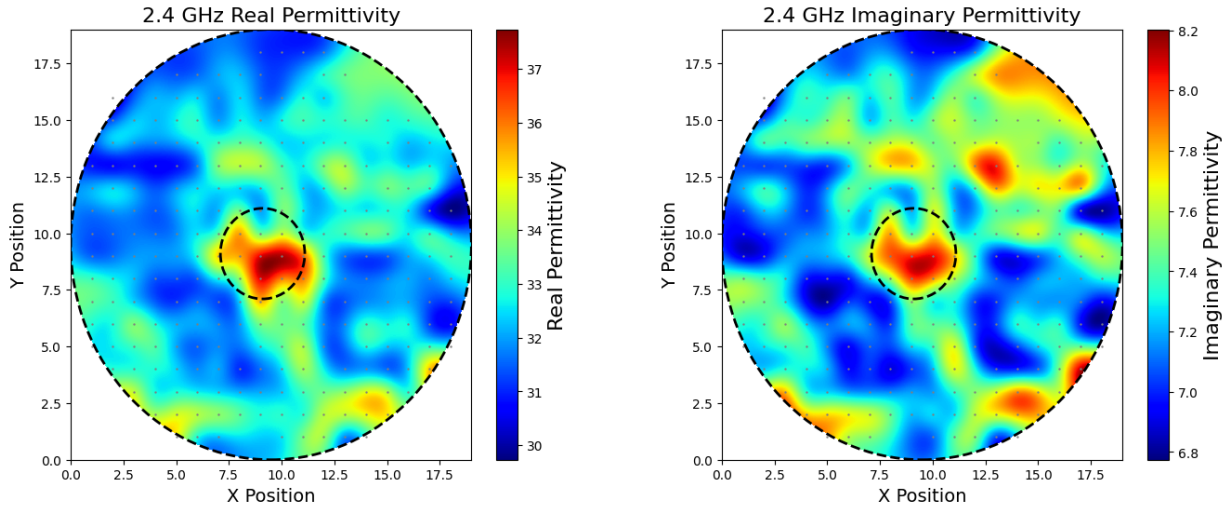

Figure 4.8: Dielectric properties at 2.4 GHz- Phantom with the skin mimic.

4.3.2 Additional Tests performed on Phantoms

Once all of the dielectric measurements on both phantoms and the corresponding permittivity maps were generated, three tests were conducted. Two tests were performed to assess the homogeneity of the fabricated phantoms, while the third test captured the

variability in repeated measurements, as three sets of measurements were taken for each phantom, with the average values plotted. The results of these tests were recorded and analysed.

Homogeneity test 1

The first homogeneity test performed on both phantoms aimed to confirm that the dimensions, as described in the Methodology section, were consistent throughout. Both phantoms were bisected, and one-half of each phantom was removed, leaving the other half to measure its depth with the stem of a Vernier calliper. For the oil-in gelatin phantom without skin mimic, the 8 mm depth of the fat layer was easily confirmed using the Vernier calliper (Figure 4.9a). In the oil-in gelatin phantom with skin mimic, the total depth of 10 mm was also verified. For a more thorough evaluation, a small portion of the phantom was removed, allowing for more detailed measurements of the skin layer, which was confirmed to be 2 mm thick (Figure 4.9b).

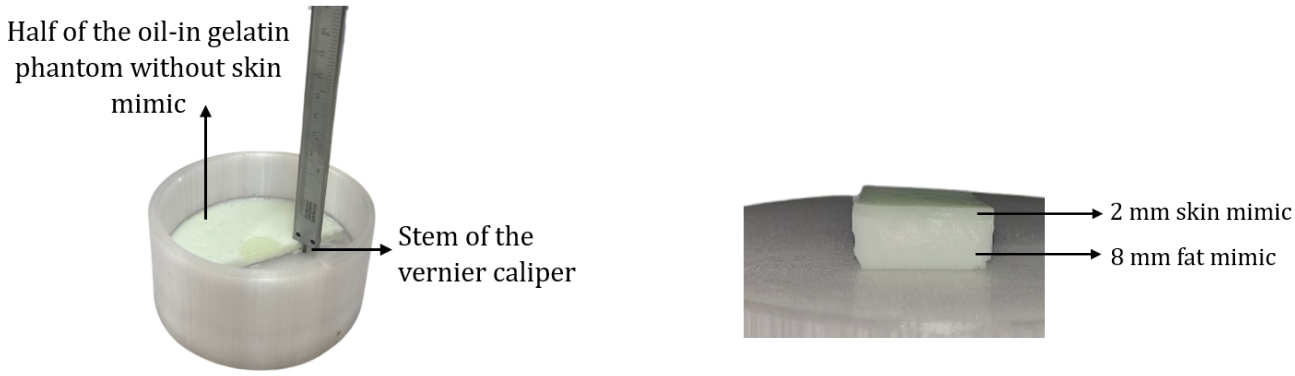

(a) Measurement of the fat layer depth in the oil-in-gelatin phantom without the skin mimic.

(b) Measurement of the skin layer in the oil-in gelatin phantom with skin mimic.

Figure 4.9: Homogeneity test 1

These measurements were taken at multiple locations across the phantom to ensure that the depth was consistent (homogeneous) throughout. The 3 mm depth of the tumour within the fat layer was confirmed during the phantom fabrication process, before em-

bedding the tumour in the coin-shaped cavity. This test confirmed that the dimensions of the phantoms were homogeneous and aligned with the planned specifications, ensuring that the depth measurements were consistent across various locations.

Homogeneity test 2

The second test evaluated the homogeneity of the dielectric properties to determine whether the same type of tissue - skin, tumour or fat- exhibited consistent dielectric properties across the surface of the phantom. Measurements of homogeneity were taken using both the phantom with the skin mimic and the phantom without the skin mimic. From the phantom without the skin mimic, measurements were randomly chosen from 8 locations directly on the fat layer and 8 locations directly on the tumour. For the phantom with the skin mimic, the dielectric measurements from 8 locations on the skin layer above the fat layer and 8 locations on the skin layer above the tumour were randomly selected. For this homogeneity test, the dielectric properties were evaluated at a single frequency of 900 MHz. The specific locations of the points chosen for each region of the phantom are presented for reference in Figure 4.10 and Figure 4.11.

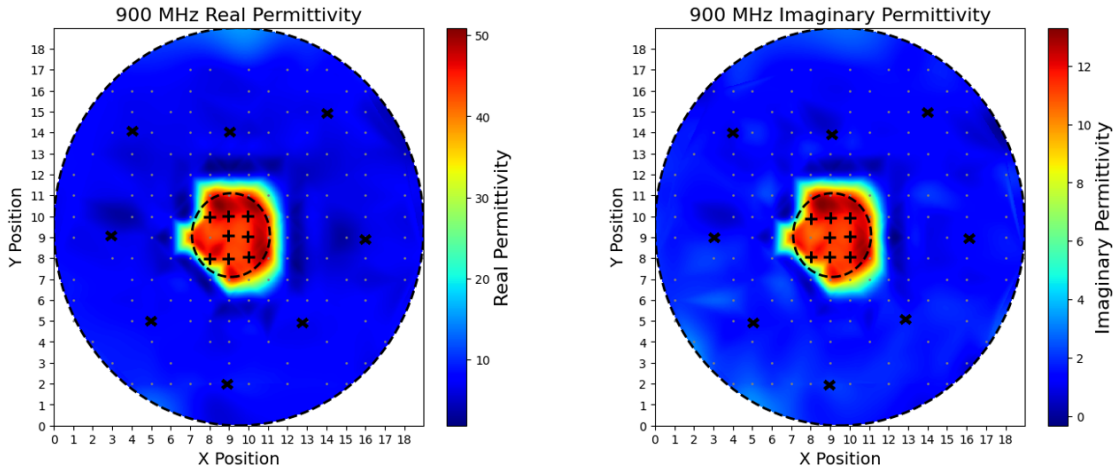

Figure 4.10: The locations randomly chosen on the phantom without skin mimic

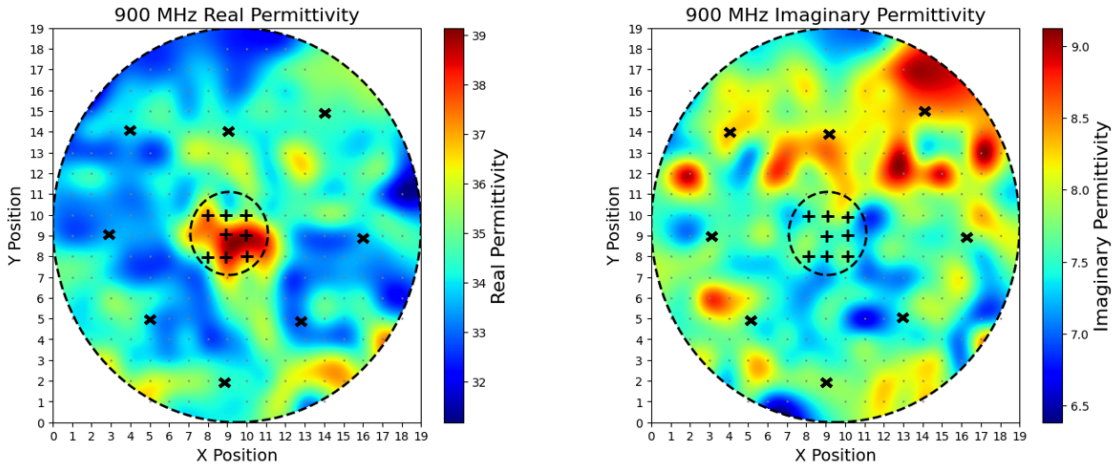

Figure 4.11: The locations randomly chosen on the phantom with skin mimic

For each region, the measurements were averaged and the standard deviation was calculated. The standard deviation was used to assess the uniformity of the dielectric properties. The results of this test, including the averaged dielectric properties and the corresponding standard deviations for each tissue type, are presented in Table 4.1.

Phantom	**Region**	**Average Real Permittivity**	**Standard Deviation (Real)**	**Average Imaginary Permittivity**	**Standard Deviation (Imaginary)**
Without skin mimic	Fat layer	10.937	±0.851	2.404	±0.387
Without skin mimic	Tumour	46.0333	±1.250	11.280	±0.453
With skin mimic	Skin layer above the fat layer	34.0521	±0.570	7.961	±0.349
With skin mimic	Skin layer above the tumour	39.259	±1.971	7.672	±0.505

Table 4.1: Assessment of the homogeneity of dielectric properties in the phantoms.

Variability in Repeated Measurements

The permittivity maps presented in Section 4.3.1 were generated after performing three separate measurements of the dielectric properties for each phantom to obtain repeated readings. The average of the three repeated readings was used to generate the final permittivity maps. This test aimed to assess the variability between the first, second, and third measurements, particularly due to the measurements being taken on different days.

Three distinct measurement locations were selected on each phantom. For the oil-in gelatin phantom without the skin mimic, the chosen locations were:

- **Location 1**: On the fat layer.
- **Location 2**: At the border between the fat layer and the tumour.
- **Location 3**: On the tumour.

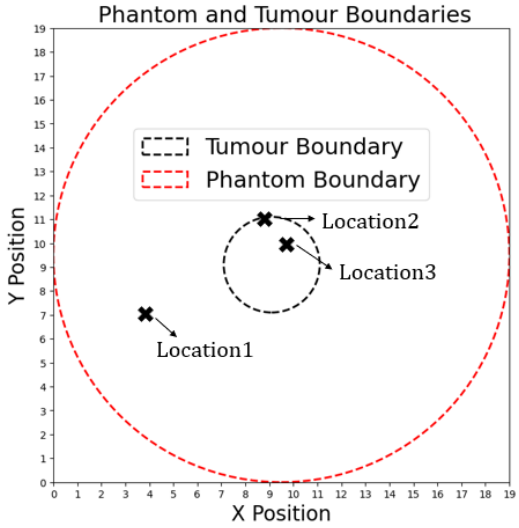

Figure 4.12: The locations chosen for the variability in repeated measurements test

For the phantom with the skin mimic, the corresponding locations were selected in the same relative positions but on the surface of the skin layer. The specific locations chosen for this test are shown in Figure 4.12.

Figure 4.13 illustrates the variability observed at Locations 1, 2, and 3 on the oil-in-gelatin phantom without skin mimic, while Figure 4.14 presents the same analysis for the oil-in-gelatin phantom with skin mimic.

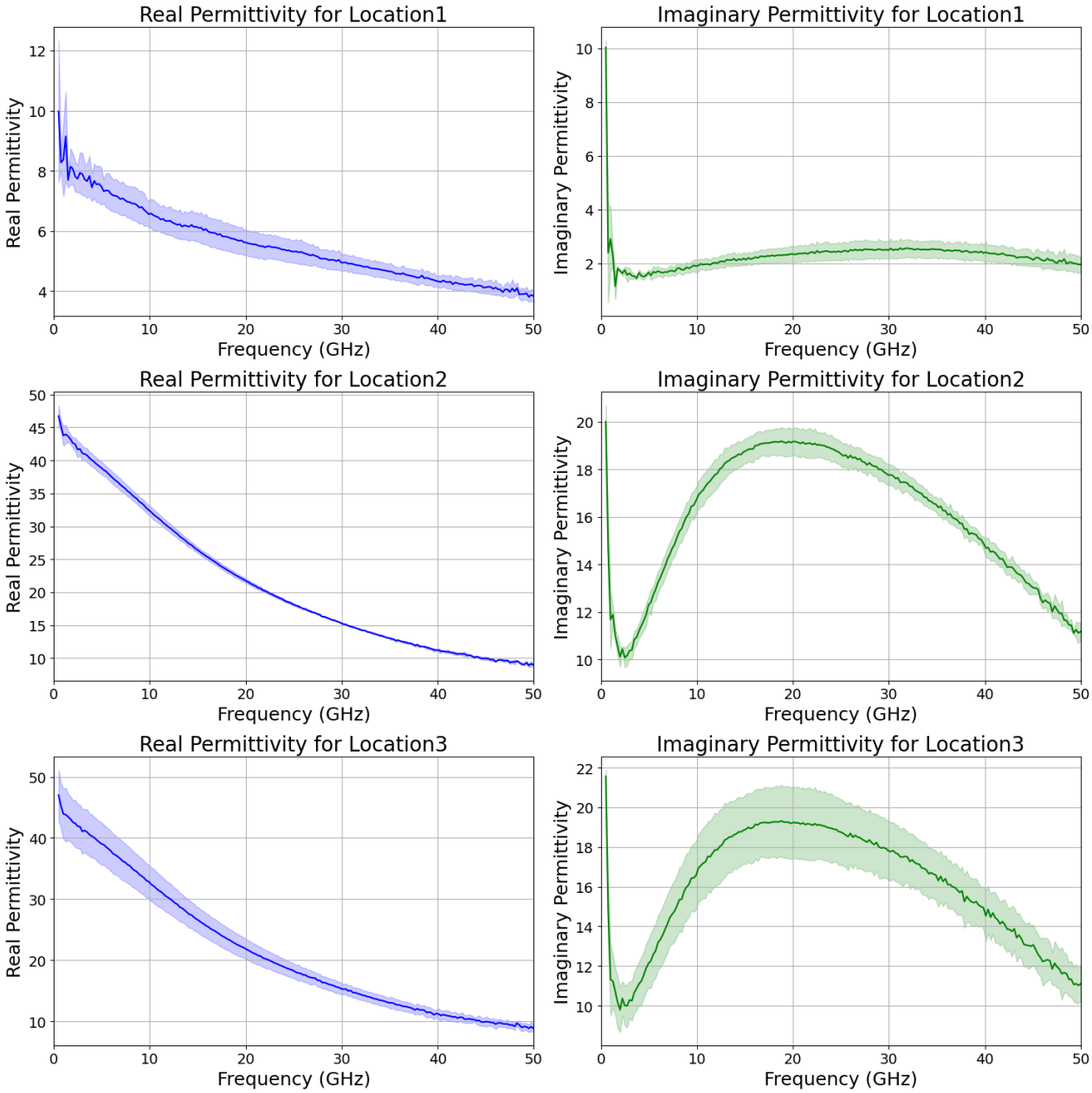

Figure 4.13: Variability in repeated measurements test - Phantom without skin mimic

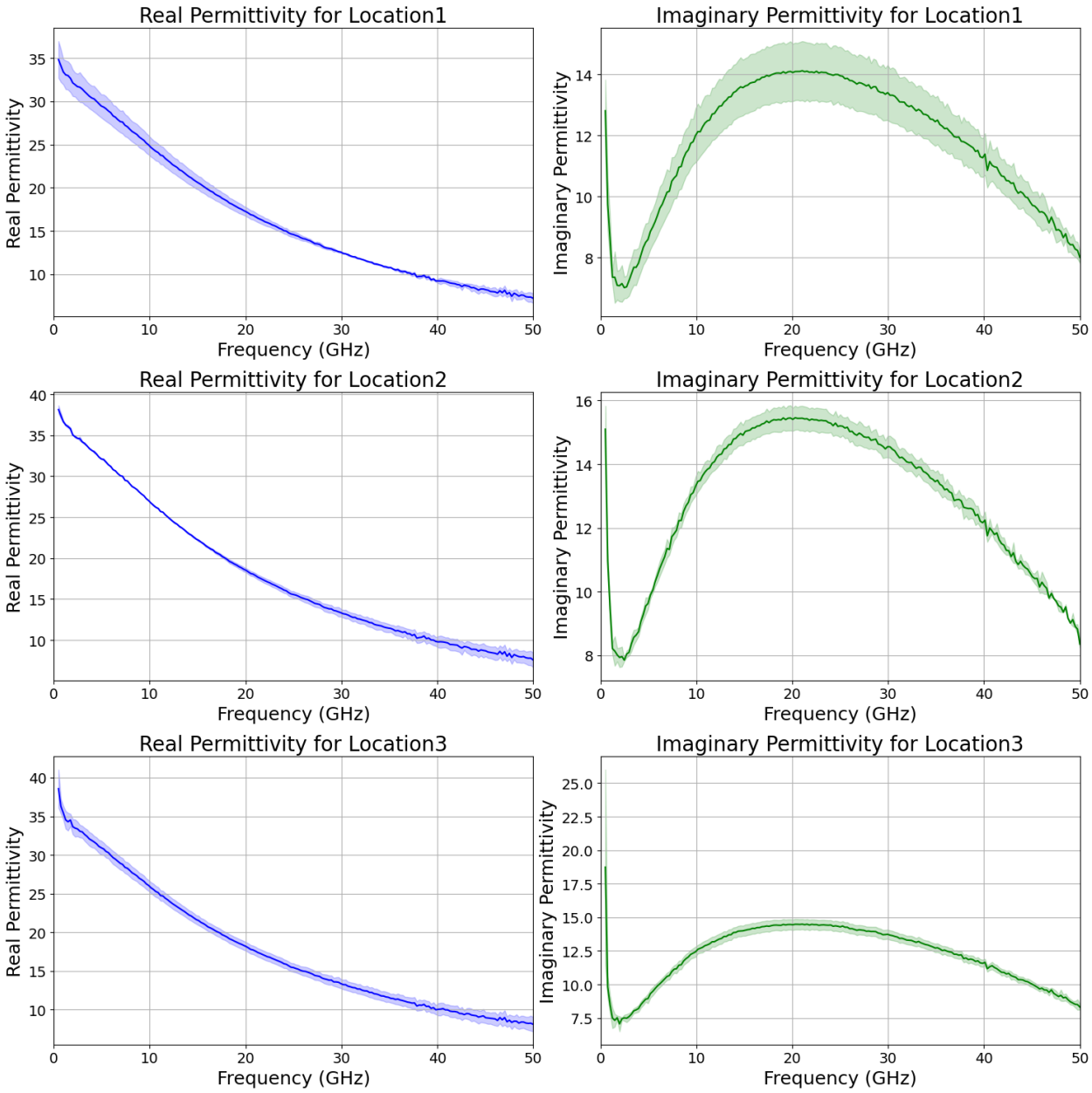

Figure 4.14: Variability in repeated measurements test - Phantom with skin mimic

4.4 Conclusion

This chapter presented the key findings of the research conducted. The following chapter provides an in-depth analysis and interpretation of these results.

CHAPTER 5

Discussion

5.1 Introduction

In this chapter, the research findings are evaluated in relation to the study objectives, with comparisons made with the existing literature.

5.2 Discussion

Microwave reflectometry techniques represent an active area of research in cancer diagnosis, particularly for detecting skin and breast tumours. Unlike other diagnostic methods, microwave and MMW imaging are non-ionising and non-invasive, making them promising tools for detecting biological abnormalities. The microwave spectrum covers frequencies from 300 MHz to 30 GHz, while MMWs operate at higher frequencies, from 30 GHz to 300 GHz.

Previous studies, such as that by Boparai and Popovic (2022), have explored the use of microwave diagnostic tools to distinguish healthy skin from lesions, focusing on frequencies up to 26.5 GHz. Limited data exist on the dielectric properties of biological tissues beyond this frequency range. This study aimed to extend current knowledge by conducting dielectric measurements at higher frequencies, specifically within the MMW spectrum (up

to 50 GHz). This study sought to evaluate their potential to improve imaging techniques based on dielectric spectroscopy.

The objectives of this research were threefold; first, to develop consistent heterogeneous phantom models that accurately depict the dielectric properties and anatomical features of skin, tumour and fat configurations; second, to extend the knowledge of dielectric properties into the MMW spectrum; and third, to analyse the impact of the skin layer on imaging based on dielectric spectroscopy for detection of skin cancer, namely liposarcoma originating in the fat below the skin surface.

The first objective aimed to delineate consistent heterogeneous phantom models that accurately depict both the dielectric properties and anatomical features of skin, tumour, and fat configurations. During Phase 2 of the study, three distinct mimics were fabricated, following the protocols highlighted in the study by Boparai and Popovic (2022), to represent the dielectric properties of skin, fat, and tumour tissue. The choice of oil-in gelatin phantoms was due to their semisolid nature, which offered stability and resistance to osmosis, making them suitable for multilayered configurations. Compared to liquid phantoms, oil-in gelatin phantoms are capable of simulating realistic situations in soft tissues, conforming to the anatomical layers required for experiments.

The oil-in gelatin phantoms were created using a combination of key ingredients as seen in Figure 3.3. Bloom gelatin served as a structural base, providing the semi-solid consistency required for stability and preventing osmosis, which makes the phantom suitable for multi-layered configurations. Sunflower was chosen as one of the primary components for the mimics, due to its dielectric properties that closely resemble those of humans. Kerosene was mixed with sunflower oil to fine-tune the dielectric constant, ensuring that the tissues would exhibit values close to those of humans. The detergent played a crucial role as an emulsifier, ensuring that the oil and water-based components were uniformly

dispersed and no separation occurred during the phantom's shelf life.

However, challenges arose during the fabrication of the fat mimic, specifically maintaining a homogeneous mixture of oil and gelatin, as seen in Figure 3.4a. This issue was particularly due to the high oil content in the fat mimic, which caused the oil to separate from the water-based gelatin mixture, making it difficult to achieve the desired uniformity. To resolve this, the gelatin mixture was stirred continuously while heated at a constant temperature of 50 °C. A pipette was used to slowly add the oil into the vortex created in the gelatin mixture, which was stirred with a magnetic stirrer (Figure 3.6b). This approach, combined with constant heating, allowed the oil to bind to the gelatin, thus preventing the separation of the layers.

A pilot study was conducted, as seen in Section 3.8.1, to compare the suitability of sunflower oil vs safflower oil, both of which are commonly used in tissue-mimicking materials. The study by Boparai and Popovic (2022) used safflower with kerosene. However, for this study, the sunflower oil-kerosene mixture was chosen as it provided more consistent dielectric values, aligned better with the target tissue properties (Figure 3.15), and proved to be more cost-effective and readily available.

Before combining these mimics into a phantom, each mimic (skin, fat and tumour) was fabricated and tested individually to ensure their dielectric properties matched those reported in the literature. To maintain the integrity of the mimics and extend their shelf life, each batch was stored in sealed plastic tubes (Figure 3.4b), minimising evaporation and preventing dehydration. This airtight storage helped ensure that the dielectric properties of the mimics would remain stable over time.

The dielectric measurements of each mimic were performed using the VNA paired with the open-ended coaxial probe (Figure 3.1), a well-established method for evaluating the dielectric properties of biological tissues. The choice of this method was informed by

its non-destructive nature and its ability to provide accurate readings across a wide frequency range. A three-step calibration process was conducted prior to each set of measurements, as discussed in Section 3.5.2. This involved calibrating the probe using air (open circuit), a shorting block, and deionised water. The calibration validation was carried out using a 0.1 mol NaCl solution, which served as a reference to verify that the probe was correctly calibrated and that the dielectric properties recorded for the known substances matched their expected values.

After calibration and validation, dielectric measurements were taken the day following the fabrication of each mimic to allow it to solidify. The dielectric properties of each mimic were measured across 201 data points ranging from 500 MHz to 50 GHz. These frequencies were chosen to cover both the microwave and millimetre wave spectrum, thereby extending the dielectric property analysis to higher frequencies where data for biological tissues are more limited. The VNA measured the S11 reflection parameter, which represents the reflected signal from the MUT. Using keysight software, the S11 parameters were converted into the material's dielectric properties, specifically the complex permittivity, in the frequency range. For each mimic, multiple measurements were taken at different depths and averaged to provide a more accurate representation of the mimic's overall dielectric properties. All measurements were performed at 0 dBm power and at room temperature.

The dielectric measurements for each mimic were represented as complex permittivity, consisting of both real and imaginary parts. These values were plotted across the frequency range of 500 MHz to 50 GHz, as can be seen in Section 4.2.1. Two subplots were generated for each mimic; the first plot displays the real part of the permittivity against the frequency, while the second plot shows the imaginary part against the frequency. The real part of the complex permittivity, or dielectric constant, represents the material's ability to store electrical energy. Higher values indicate greater polarisation in response to the

electric field. The imaginary part relates to dielectric losses, showing how much energy is dissipated as heat. For each mimic, these plots were also compared with existing literature (Section 4.2.1), providing a complete view of how the measured dielectric properties aligned with previously reported values for biological tissues.

The dielectric properties of the skin mimic were compared with the data provided by Gabriel et al. (1996), which included measurements of wet and dry skin up to 20 GHz and extrapolated using the Cole-Cole model up to 100 GHz. The results of the skin mimic showed strong agreement with the literature, particularly with the wet skin model, for both the real and imaginary parts of the permittivity. The real part exhibited a decreasing trend as frequency increased, which is consistent with the expected behaviour of biological tissues. This close alignment suggested that the skin mimic accurately captured the dielectric behaviour of the skin in the microwave and MMW spectrum. As shown in Figure 4.1a, this agreement is visible throughout the full frequency range. The imaginary part also showed a pattern similar to that in the literature, with minor deviations at lower frequencies where the mimic exhibited slightly lower values compared to both wet and dry skin. However, overall, the mimic performed well in simulating skin tissue across the frequency range.

The shelf life of the skin mimic was tested over a period of 24 weeks, during which it remained stable (Figure 4.1b). This stability highlights the importance of proper storage conditions, as the mimics were sealed in airtight plastic tubes to prevent evaporation or dehydration, thereby preserving the dielectric properties over time. Additionally, reproducibility tests were conducted and confirmed that the mimic could be easily re-fabricated with consistent dielectric properties, ensuring that the oil-in gelatin phantom could be reliably used in subsequent experiments (Figure 4.1c). For each set of measurements presented in this study, standard deviations were calculated to account for variations in repeated readings.

The dielectric properties of the fat mimic were also compared with the data provided by Gabriel et al. (1996), as shown in Figure 4.3a. The real part of the permittivity showed good agreement with the literature's data across the entire frequency range, although the mimic consistently displayed slightly higher values, particularly at lower frequencies. The imaginary part also closely followed the trend observed in the literature, with the fat mimic showing slightly elevated values at lower frequencies. Despite these differences, the overall results confirmed that the fat mimic behaved in a manner consistent with biological fat, validating its use in this study. The shelf life of the fat mimic was assessed over a period of 24 weeks, as seen in Figure 4.3b. The results indicated that the mimic remained stable for up to 8 weeks, showing consistent dielectric properties during this time. However, noticeable variations in both the real and imaginary parts of the permittivity were observed from 16 weeks onwards with increasing deviation from the initial measurements. The higher oil content in the fat mimic may have contributed to its limited shelf life by affecting the balance between the oil and water components, potentially leading to dehydration or phase separation over time. Additionally, a reproducibility test was also conducted to ensure that the fat mimic could be easily replicated with consistent dielectric properties (Figure 4.3c). The test showed that the newly fabricated fat mimic closely matched the original, confirming that the fabrication process could be reliably reproduced. The small deviations seen in the reproducibility test fell within the acceptable range, further supporting the mimic's suitability for future phantom models. Repeated readings were also taken, and standard deviations were calculated for each measurement.

The results of the tumour mimic showed strong alignment with both Lazebnik et al. (2007) and Martellosio et al. (2016) (Figure 4.2a). The mimic closely followed the trends observed in both studies, with only minor deviations, further validating the accuracy of the fabricated mimic. Lazebnik's study, which provided data up to 20 GHz, was particularly well matched to the mimic, reflecting its ability to replicate the properties of tumour tis-

sue within that frequency range. The imaginary part, associated with dielectric losses, showed a similar overall trend, but the lab results indicated slightly lower values at lower frequencies when compared to both Lazebnik and Martellosio's results. The shelf life tests showed that the dielectric properties of the tumour mimic remained stable over 24 weeks, with slight variations, especially in the real permittivity, after 16 weeks, possibly due to dehydration. Reproducibility tests demonstrated that the tumour mimic could be reliably fabricated with similar dielectric properties.

From these mimics, it can be concluded that the permittivity of tissues with lower water content, such as fat, is significantly lower than those with higher water content, such as tumours. All the results mentioned above extended dielectric properties up to 50 GHz, into the MMW spectrum. Once the dielectric properties of each mimic were validated against existing literature, the oil-in gelatin phantoms were fabricated, as detailed in Section 3.6.2.

3D printing was used in the fabrication process, allowing for the creation of essential components such as the outer casing and the design of the coin-shaped hollow for tumour insertion. Using Fusion 360 software, the designs were modelled and printed with PETG, a water-resistant material. Two different designs were evaluated in separate pilot studies for the creation of the coin-shaped hollow for tumour insertion (Section 3.8.3). The chosen design (Figure 3.7) was more stable, less prone to human error, and functioned as a lid while the fat mimic solidified, offering better protection from exposure to air and temperature changes. Before incorporating the tumour insertion design into the 8 mm fat layer, calculations were carried out to ensure that inserting the tumour component would not increase the fat layer's thickness. The calculations showed a depth increase of 0.12 mm, which was considered negligible. After completing the 3D printing process and following the procedure detailed in Section 3.6.2 for the fabrication of oil-in gelatin phantoms, two phantoms were successfully fabricated, as shown in Figure 4.4.

As seen in Figure 4.4, one of the phantoms included a 2 mm thick skin layer on top of the fat layer with the tumour embedded, while the other phantom consisted only of the fat layer with the embedded tumour. This allowed the study to evaluate the effect of the skin layer on dielectric imaging for liposarcoma detection. Once fabricated, the phantoms were stored in plastic wrap to ensure airtight sealing.

In addition to the phantoms, some of the mixtures were poured into separate plastic tubes, allowing for dielectric property measurements. This ensured that the properties remained consistent with the results obtained in Phase 2 and aligned with the existing literature. After confirmation that the dielectric properties were correct, fabrication was validated and Phase 4 began, which involved measurements on the two phantoms. Section 3.7, gives a detailed description of how measurements of dielectric properties were taken on both phantoms.

Measurements with the VNA and the open-ended coaxial probe were taken on both phantoms using the 3D printed grid, as seen in Figure 3.13a. The 3D printed grid helped to ensure precise positioning of the probe. With each square spaced 2 mm apart, this provided a good spatial resolution of the phantom's surface. The dimensions of each square (3 mm by 3 mm) also helped minimise probe movement. As seen in Figure 3.13b, the phantom remained stationary during the measurements with the help of a G-clamp and double-sided tape. For each location, three repeated readings were taken on different days.

During the measurements, a constant power of 0 dBm was used. Low-power microwave reflectometry has been shown in the existing literature to enhance sensitivity [Mirbeik-Sabzevari and Tavassolian, 2018], offering the potential for early-stage cancer detection. Proper probe contact was ensured by applying light pressure against the surface during measurements, minimising the risk of air pockets forming between the probe tip and the phantom. To maintain consistency, the probe was carefully marked to ensure

it was inserted to the same depth in all measurements, maintaining uniform pressure and depth. The literature supports the idea that as long as proper contact is maintained, variations in pressure do not significantly affect the reflection coefficient [Mehta et al., 2006].

The measurements recorded for the three consecutive readings for each phantom were averaged, and the results were presented as permittivity maps. Although the measurements were discrete, radial basis function interpolation was used to generate a smooth surface between the data points. This method also allowed for extrapolation, estimating dielectric properties in regions beyond the measured points. This created a continuous and smooth representation of the dielectric profile across the phantom's surface. By analysing the permittivity maps of the phantom without and with the skin layer, the third objective of this study was achieved.

Figure 4.5 presents the permittivity maps for the phantom without skin. At all three frequencies (900 MHz, 25 GHz and 50 GHz), the tumour region exhibited significantly higher permittivity values, both real and imaginary, compared to surrounding fat tissue. This contrast is due to the higher water content of the tumour, a characteristic that microwave reflectometry exploits effectively. The higher dielectric properties in the tumour were consistent across all frequency ranges, with both real and imaginary permittivity showing distinct regions of contrast. The permittivity maps showed that the location and shape of the tumour could be reasonably detected for the three different frequencies, with the tumour appearing approximately circular and positioned within its actual contour. Although the boundary of the tumour was not sharply defined and the tumour appeared to "spill over" into adjacent areas, this was attributed to averaging and the limitations in spatial resolution. The size of the tumour, when evaluated in relation to the 3D printed grid, was closely aligned with the real dimensions. Given that each square in the grid was 3 mm with 2 mm spacing, a total of 5 mm per step, and the tumour spanned roughly four squares in both the x- and y- directions, this confirmed a tumour diameter of ap-

proximately 20 mm, consistent with its actual size. A more precise representation could potentially have been obtained by using a robotic arm, which would offer finer resolution by allowing measurements at smaller increments than the 5 mm grid spacing. As the frequency increased from 900 MHz to 50 GHz, the real permittivity values decreased throughout the phantom. This is consistent with the known behaviour of biological tissues, where dielectric properties tend to decrease at higher frequencies. Similarly, the imaginary permittivity values followed a similar trend of decreasing with increasing frequency.

The dielectric properties of both the tumour and the fat regions slightly decreased when measured compared to the values obtained immediately after fabrication (Figure 3.12). This reduction could be due to the larger surface area of the phantom compared to the smaller plastic tubes used in earlier measurements, leading to increased evaporation and thus, dehydration. Furthermore, while the phantom was sealed using plastic wrap, it was not as tightly sealed as the plastic tubes, likely contributing to loss of moisture. The use of PETG, although watertight, may have absorbed some of the water content over time, which could have led to a reduction in dielectric properties.

Thus, for the phantom without the skin, the tumour was successfully detected across all frequency ranges, demonstrating sufficient contrast for both microwave and millimetre waves. The contrast was more pronounced at lower frequencies (microwaves). The tumour's shape and size were identified, confirming that microwave reflectometry and MMW techniques are both effective in detecting the presence and extent of the tumour.

Figure 4.6 presents the permittivity maps for the phantom with skin. The primary challenge in detecting the tumour was that the skin and tumour have very similar dielectric properties, making differentiation difficult. At 900 MHz, the range of contrast in permittivity was narrow, with real permittivity values ranging from around 32 to 39 and imag-

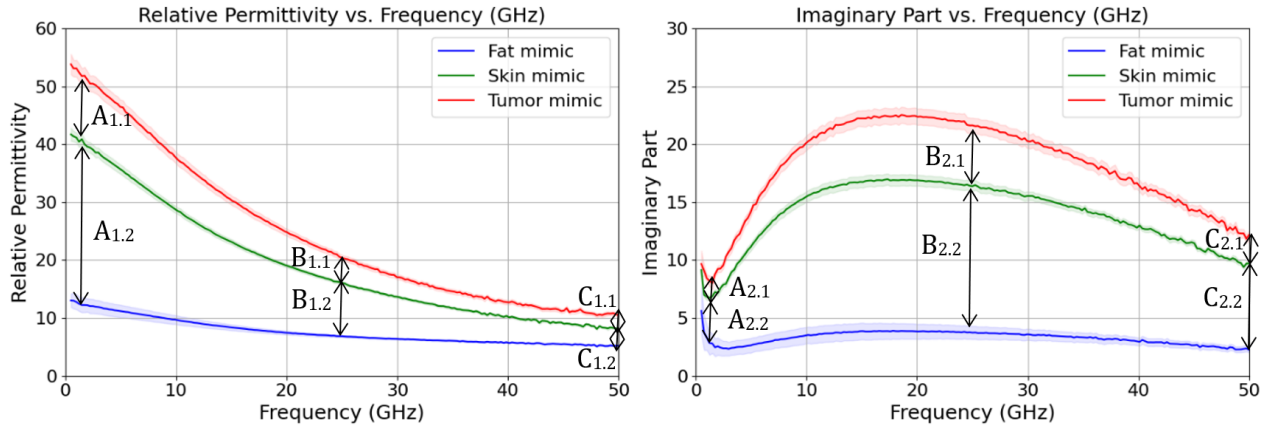

Figure 5.1: Difference in dielectric properties between skin and tumour and skin and fat.

inary permittivity values from around 6.5 to 9. The tumour was detected in the real permittivity at 900 MHz, as there is a notable difference in dielectric properties between the skin and tumour (Figure 5.1- arrow $A_{1.1}$) and skin and fat (Figure 5.1- arrow $A_{1.2}$). However, in the imaginary permittivity, the properties are much closer (Figure 5.1- arrows $A_{2.1}$ and $A_{2.2}$) and the tumour was not detected. Although the tumour was identified within the dashed contour in the real permittivity, the precise size and shape could not be determined. These findings suggested the presence of a tumour but did not provide definitive confirmation of its exact dimensions or morphology.

At 25 GHz, the tumour was detected in both the real and imaginary parts, as there was still contrast between the dielectric properties of the skin and tumour (Figure 5.1- arrows $B_{1.1}$ and $B_{2.1}$ respectively) and skin and fat (Figure 5.1- arrows $B_{1.2}$ and $B_{2.2}$ respectively). As shown in both Figure 4.6 and Figure 5.1, the contrast in the imaginary permittivity was greater, which led to more effective detection of the tumour in this parameter. However, the shape and size were not clearly resolved.

At 50 GHz, even though in the MMW spectrum, there was sufficient penetration depth. Thus, given that the skin layer was only 2 mm thick, there was enough penetration for

the tumour to be detected. However, the tumour was only detected in the imaginary permittivity. It was not detected in the real permittivity, possibly because the contrast between the skin and tumour and skin and fat in the real part (as seen in Figure 5.1 - arrows $C_{1.1}$ and $C_{1.2}$ respectively) was too small. The contrast in the imaginary part was larger (as seen in Figure 5.1 - arrows $C_{2.1}$ and $C_{2.2}$), allowing for detection. The ability to detect the tumour largely depended on the contrast between the dielectric properties of the different tissue types at each frequency. However, even though in some permittivity maps, the tumour was detected no further information regarding its shape and size could be concluded.

Figures 4.7 and 4.8 present the permittivity maps for the dielectric properties of the phantoms without the skin mimic and with the skin mimic at 2.4 GHz, respectively. This frequency was chosen as it falls within the ISM band, making it particularly relevant for medical imaging applications. In the phantom without the skin mimic, the tumour is easily detectable, with significant contrast between the tumour and the surrounding fat, allowing the shape and size of the tumour to be clearly discerned. For the phantom with the skin mimic, while the tumour was still detected in the real permittivity, its shape and size were less noticeable. However, an elevated dielectric property at the centre indicated the presence of the tumour. In the imaginary part, elevated dielectric measurements were also observed outside the tumour region, reducing its reliability for accurate tumour detection.

From these findings, it can be concluded that liposarcoma beneath a 2 mm thick skin layer can be detected using both microwave frequencies (mainly through real permittivity) and MMW frequencies (mainly through imaginary permittivity). Although the presence of skin impacted the detection accuracy, making it more difficult to precisely define the tumour‘s shape and size, the tumour was still noticeable. At MMW frequencies, sufficient penetration was achieved, and despite the similar dielectric properties between the skin

and tumour, the presence of the tumour was still detectable. Without the skin, the tumour's shape and size were more clearly detected. This demonstrated the potential for microwave and MMW techniques to detect liposarcoma.

After all measurements were recorded and evaluated, two homogeneity tests were performed to ensure uniformity in both the dimensions and dielectric properties of the phantoms. The first test, detailed in Section 4.3.2, focused on evaluating the homogeneity of the dimensions across the different layers in the multi-layer phantoms. The result confirmed that the phantoms were consistent throughout, with an 8 mm fat layer, 2 mm skin layer, and the tumour embedded 3 mm deep within the fat layer. Thus, the dimensions aligned with the intended design specifications, making the phantom homogeneous. The second test, also detailed in Section 4.3.2, was performed to evaluate the homogeneity of the dielectric properties in the same regions of the phantoms. Table 4.1 presented the standard deviation for each region in both phantoms. The standard deviation values were small across all measurements, indicating minimal variation in dielectric properties at different locations within the same region. From Table 4.1, it can be concluded that the dielectric properties were consistent across the phantom, the largest deviation being ± 1.250 in the tumour region of the phantom without the skin mimic. These results confirmed that the dielectric properties were uniform within each region, demonstrating the overall homogeneity of the phantoms.

A third test was conducted to evaluate the variability in the three repeated dielectric measurements for each phantom. Although the average of these readings was used for the permittivity maps, the standard deviation provided insight into the consistency of the repeated measurements. Three distinct locations were selected for each phantom, representing different regions. The selection of these regions was informed by the results of the second test, which confirmed that each region exhibited homogeneity. As the measurements were taken on different days, it was important to ensure that dehydration or

evaporation did not alter the dielectric properties, despite the phantom being sealed with plastic wrap. Standard deviation plots were generated for each region, showing the average measurement and variability. The largest deviation occurred at location 3 (Figure 4.12) in the phantom without skin (on the tumour), likely due to the evaporation of water from the tumour's high water content. A smaller variation was observed at Location 1 on the skin-covered phantom. A comparison of Figures 4.13 and 4.14 showed less variability in the phantom with skin, suggesting that the skin layer may have acted as a protective barrier, preserving the dielectric properties. Overall, the variability was minimal, confirming the reliability of dielectric properties across the repeated measurements.

In conclusion, this discussion demonstrated that all three study objectives were successfully achieved. Consistent heterogeneous phantoms were fabricated, accurately replicating the dielectric properties of skin, tumour, and fat. The dielectric properties were measured up to 50 GHz, aligning well with the extrapolated models from the literature. Furthermore, the effect of a 2 mm skin layer was evaluated, confirming that the presence of a tumour can still be detected using microwave techniques focusing mainly on real permittivity and MMW techniques focusing on the imaginary permittivity.

5.3 Conclusion

This chapter has provided a comprehensive analysis and interpretation of the findings of this study. The following chapter will focus on presenting the conclusions drawn from this research and providing recommendations for professional practice and future research.

CHAPTER 6

Conclusions and Recommendations

6.1 Introduction

This chapter presents the key findings from the research, along with practical recommendations for professional application and suggestions for future research.

6.2 Summary of Conclusions from the Study

The following section outlines the key conclusions derived from this research.

1. **Phantom fabrication:**

   The research demonstrated the fabrication of consistent heterogeneous phantoms that accurately replicated the dielectric properties of skin, fat and tumour tissues. The phantoms were confirmed to be homogeneous in both dimensions and dielectric properties within the same tissue type, ensuring uniformity across all layers. The phantom's design created a stable multilayered structure with minimal osmosis occurring between layers, preserving the integrity of the mimic materials. The skin, fat, and tumour mimics were all fabricated using the same base ingredients, but in different concentrations to replicate their respective dielectric properties. The ingredients used were readily available, making it feasible for future research.

2. **Dielectric measurements:**
   Dielectric properties were extended up to 50 GHz, confirming the expected behaviour of tissues over a wide frequency range, including the MMW spectrum. These properties were consistent with existing models in the literature.

3. **Skin layer effect on producing images based on dielectric spectroscopy:**
   This study evaluated the impact of the 2 mm skin layer on tumour detection. Despite the similarities in the dielectric properties of skin and tumour, the tumour remained detectable using microwave and MMW reflectometry techniques. In the microwave range, focusing on the real part of the permittivity indicated the tumour's presence, while in the MMW range the imaginary permittivity provided more effective detection. The tumour was not detected at 900 MHz in the imaginary part and at 50 GHz in the real part. This could be due to the similarities of the dielectric properties of skin and tumour at those frequencies, thus not providing enough contrast for the tumour to be detected. The presence of the skin diminished the clarity of the tumour's shape and size. Without the skin layer, the tumour's shape and size were more accurately defined in both the real and imaginary part of the permittivity, but this was reduced when a 2 mm skin layer was present.

6.3 Recommendations for Professional Practice

The results of this study lead to several important recommendations for professional practice in medical physics, specifically concerning cancer detection through microwave and MMW reflectometry.

1. **Implementation of non-invasive technologies in clinical settings:**
   This study has demonstrated that both microwaves and MMW can be used for detecting liposarcoma with minimal invasion. It is recommended that these non-

ionising technologies be incorporated into clinical practice, especially for early-stage cancer detection, thereby reducing the need for more invasive or ionising procedures.

2. **Quality Assurance Protocols for phantoms:**
   Although the oil-in gelatin phantoms have demonstrated a reasonably good shelf life, it is critical for medical physicists to establish and standardise quality assurance protocols for these phantoms, ensuring they meet European standards. Research should be conducted to explore methods to extend the shelf life of oil-in gelatin phantoms to make them more suitable for prolonged clinical use.

3. **Development of Training Modules for Medical Professionals:**
   Medical physicists should take an active role in developing training programs that focus on the practical applications of dielectric spectroscopy in clinical diagnostics. This will also ensure that the technology reaches its full potential, possibly identifying new applications both for diagnosis and treatment Using phantom models to simulate clinical scenarios, these training modules would enable healthcare professionals to gain proficiency in interpreting data from microwave and MMW imaging systems.

6.4 Recommendations for Future Research

Based on the findings of this study, the following recommendations are proposed for future research:

1. Extending the frequency range up to 90 GHz would allow a deeper evaluation of the MMW spectrum, potentially improving tumour detection, and further investigating dielectric properties at higher frequencies.

2. Future experiments could benefit from using a robotic arm to perform the measure-

ments. This would improve spatial resolution and potentially provide clearer detection of tumour boundaries and shapes, addressing the limitations observed with the 3D printed grid.

3. The same study should be repeated by varying the thickness of the skin layer to provide more comprehensive insight into how different skin thicknesses affect imaging and tumour detection.

4. Research can be conducted based on this study, however, exploring the effects of varying tumour size and tumour depth within the fat layer to evaluate the impact of tumour dimensions on detectability and imaging clarity.

5. Expanding this study to include other types of skin cancer beyond liposarcoma would provide a more robust understanding of how dielectric spectroscopy performs on different types of cancer, leading to broader clinical relevance.

6.5 Conclusion

This study successfully achieved its three main objectives. The fabrication of consistent heterogeneous phantoms that accurately replicated the dielectric properties of skin, fat, and tumour tissue was accomplished, with uniformity confirmed in both dimensions and dielectric properties. The dielectric measurements extended into the MMW spectrum up to 50 GHz, aligning with the existing literature and contributing valuable data at higher frequencies.

The effect of a 2 mm skin layer on tumour detection was evaluated by fabricating two phantoms, with and without the skin layer. Despite the similar dielectric properties of skin and tumour, the tumour was detectable, though the presence of the skin reduced clarity in defining its shape and size. This research demonstrated the potential of dielectric spectroscopy for non-invasive tumour detection, particularly for skin cancer.

References

Akkus, O., Oguz, A., Uzunlulu, M., Kizilgul, M., et al. (2012). Evaluation of skin and subcutaneous adipose tissue thickness for optimal insulin injection. *J Diabetes Metab*, 3(8):2.

Alabaster, C. (2003). Permittivity of human skin in millimetre wave band. *Electronics Letters*, 39(21):1.

Alborova, I. L., Bonello, J., Farrugia, L., Sammut, C. V., and Anishchenko, L. N. (2017). A study of the dielectric properties of biological tissues: ex-vivo vs preserved samples. In *2017 Progress In Electromagnetics Research Symposium-Spring (PIERS)*, pages 2373–2377. IEEE.

Aminzadeh, R., Saviz, M., and Shishegar, A. A. (2014). Dielectric properties estimation of normal and malignant skin tissues at millimeter-wave frequencies using effective medium theory. In *2014 22nd Iranian Conference on Electrical Engineering (ICEE)*, pages 1657–1661. IEEE.

Barnes, F. S. and Greenebaum, B. (2018). *Biological and medical aspects of electromagnetic fields*. CRC press.

Boparai, J., Kranold, L., Fortaleza, L., and Popović, M. (2020). Dielectric properties of skin-mimicking tissue models in the 5–20 ghz range. In *2020 IEEE International Sympo-*

sium on Antennas and Propagation and North American Radio Science Meeting, pages 1623–1624. IEEE.

Boparai, J. and Popović, M. (2022a). Development and characterization of skin phantoms at microwave frequencies. *IEEE Journal of Electromagnetics, RF and Microwaves in Medicine and Biology*, 6(3):296–304.

Boparai, J. and Popović, M. (2022b). Heterogeneous skin phantoms for experimental validation of microwave-based diagnostic tools. *Sensors*, 22(5):1955.

Chahat, N., Zhadobov, M., and Sauleau, R. (2012). Broadband tissue-equivalent phantom for ban applications at millimeter waves. *IEEE Transactions on Microwave Theory and Techniques*, 60(7):2259–2266.

Farrugia, L., Wismayer, P. S., Mangion, L. Z., and Sammut, C. V. (2016). Accurate in vivo dielectric properties of liver from 500 mhz to 40 ghz and their correlation to ex vivo measurements. *Electromagnetic biology and medicine*, 35(4):365–373.

Gabriel, S., Lau, R., and Gabriel, C. (1996). The dielectric properties of biological tissues: Iii. parametric models for the dielectric spectrum of tissues. *Physics in medicine & biology*, 41(11):2271.

Garrett, J. and Fear, E. (2014). Stable and flexible materials to mimic the dielectric properties of human soft tissues. *IEEE Antennas and Wireless Propagation Letters*, 13:599–602.

Hwang, H., Yim, J., Cho, J.-W., Cheon, C., and Kwon, Y. (2003). 110 ghz broadband measurement of permittivity on human epidermis using 1 mm coaxial probe. In *IEEE MTT-S International Microwave Symposium Digest, 2003*, volume 1, pages 399–402. IEEE.

Joseph, L., Asan, N. B., Ebrahimizadeh, J., Chezhian, A. S., Perez, M. D., Voigt, T., and Augustine, R. (2020). Non-invasive transmission based tumor detection using anthropo-

morphic breast phantom at 2.45 ghz. In *2020 14th European Conference on Antennas and Propagation (EuCAP)*, pages 1–5. IEEE.

Joseph, L., Perez, M. D., and Augustine, R. (2018). Development of ultra-wideband 500 mhz–20ghz human skin phantoms for various microwaves based biomedical applications. In *2018 IEEE Conference on Antenna Measurements & Applications (CAMA)*, pages 1–3. IEEE.

Kazemi, F., Mohanna, F., and Ahmadi-Shokouh, J. (2018). Detection of biological abnormalities using a near-field microwave microscope. *International Journal of Microwave and Wireless Technologies*, 10(8):933–941.

Keysight Technologies (2020). *Keysight 85070E Dielectric Probe Kit*.

Kharkovsky, S. and Zoughi, R. (2007). Microwave and millimeter wave nondestructive testing and evaluation-overview and recent advances. *IEEE Instrumentation & Measurement Magazine*, 10(2):26–38.

Khuda, I. E. (2017). A comprehensive review on design and development of human breast phantoms for ultra-wide band breast cancer imaging systems. *Engineering Journal*, 21(3):183–206.

La Gioia, A., Porter, E., Merunka, I., Shahzad, A., Salahuddin, S., Jones, M., and O'Halloran, M. (2018). Open-ended coaxial probe technique for dielectric measurement of biological tissues: Challenges and common practices. *Diagnostics*, 8(2):40.

Lazebnik, M., Popovic, D., McCartney, L., Watkins, C. B., Lindstrom, M. J., Harter, J., Sewall, S., Ogilvie, T., Magliocco, A., Breslin, T. M., et al. (2007). A large-scale study of the ultrawideband microwave dielectric properties of normal, benign and malignant breast tissues obtained from cancer surgeries. *Physics in medicine & biology*, 52(20):6093.

Marsland, T. and Evans, S. (1987). Dielectric measurements with an open-ended coaxial probe. In *IEE proceedings H (microwaves, antennas and propagation)*, volume 134, pages 341–349. IET.

Martellosio, A., Pasian, M., Bozzi, M., Perregrini, L., Mazzanti, A., Svelto, F., Summers, P. E., Renne, G., Preda, L., and Bellomi, M. (2016). Dielectric properties characterization from 0.5 to 50 ghz of breast cancer tissues. *IEEE Transactions on Microwave Theory and Techniques*, 65(3):998–1011.

Mehta, P., Chand, K., Narayanswamy, D., Beetner, D. G., Zoughi, R., and Stoecker, W. V. (2006). Microwave reflectometry as a novel diagnostic tool for detection of skin cancers. *IEEE Transactions on Instrumentation and Measurement*, 55(4):1309–1316.

Mirbeik-Sabzevari, A., Ashinoff, R., and Tavassolian, N. (2017). Ultra-wideband millimeter-wave dielectric characteristics of freshly excised normal and malignant human skin tissues. *IEEE Transactions on Biomedical Engineering*, 65(6):1320–1329.

Mirbeik-Sabzevari, A. and Tavassolian, N. (2018). Ultrawideband, stable normal and cancer skin tissue phantoms for millimeter-wave skin cancer imaging. *IEEE Transactions on Biomedical Engineering*, 66(1):176–186.

Mirbeik-Sabzevari, A. and Tavassolian, N. (2019). Tumor detection using the millimeter-wave technology.

Oliveira, B. L., Godinho, D., O'Halloran, M., Glavin, M., Jones, E., and Conceição, R. C. (2018). Diagnosing breast cancer with microwave technology: Remaining challenges and potential solutions with machine learning. *Diagnostics*, 8(2):36.

Pethig, R. (1987). Dielectric properties of body tissues. *Clinical Physics and Physiological Measurement*, 8(4A):5.

Porter, E., Fakhoury, J., Oprisor, R., Coates, M., and Popović, M. (2010). Improved tissue phantoms for experimental validation of microwave breast cancer detection. In *Proceedings of the fourth European conference on antennas and propagation*, pages 1–5. IEEE.

Ruvio, G., Solimene, R., Cuccaro, A., Browne, J., Gaetano, D., and Ammann, M. (2013). Experimental microwave breast cancer detection with oil-on-gelatin phantom. In *2013 International Conference on Electromagnetics in Advanced Applications (ICEAA)*, pages 871–874. IEEE.

Ruvio, G., Vaselli, M., Lopresto, V., Pinto, R., Farina, L., and Cavagnaro, M. (2018). Comparison of different methods for dielectric properties measurements in liquid sample media. *International Journal of RF and Microwave Computer-Aided Engineering*, 28(3):e21215.

Saponara, M., Stacchiotti, S., and Gronchi, A. (2017). Pharmacological therapies for liposarcoma. *Expert Review of Clinical Pharmacology*, 10(4):361–377.

Sasaki, K., Wake, K., and Watanabe, S. (2014). Measurement of the dielectric properties of the epidermis and dermis at frequencies from 0.5 ghz to 110 ghz. *Physics in Medicine & Biology*, 59(16):4739.

Topfer, F. and Oberhammer, J. (2015). Millimeter-wave tissue diagnosis: The most promising fields for medical applications. *IEEE Microwave Magazine*, 16(4):97–113.

Venkatesh, M. and Raghavan, G. (2005). An overview of dielectric properties measuring techniques. *Canadian biosystems engineering*, 47(7):15–30.

Vorlıcek, J., Oppl, L., and Vrba, J. (2010). Measurement of complex permittivity of biological tissues. *Progress In Electromagnetics Research*, 599.

APPENDIX A

Appendix

Python Code:

```
# -*- coding: utf-8 -*-
"""heatmapscode

Automatically generated by Colab.

Original file is located at
    https://colab.research.google.com/drive/1
        cQ3cjk8yKb380TaaWSAurbSnR3DXIcMB
"""

import numpy as np
import matplotlib.pyplot as plt
import glob
import os
from scipy.interpolate import Rbf
from matplotlib.patches import Circle

# Function to read data
def read_data(filename):
    with open(filename, 'rb') as f:
```

```
        data = np.loadtxt(f, skiprows=1)
        if data.ndim == 1 or data.size == 0:
            print(f"File {filename} contains insufficient data.")
            return None
        return data

# Function to extract coordinates from the filename
def extract_coordinates(filename):
    coords = os.path.splitext(filename)[0].split('.')
    if len(coords) == 2:
        return float(coords[0]), float(coords[1])
    else:
        print(f"Filename {filename} is not in the correct format.")
        return 0.0, 0.0

# Functions for extracting the desired data (e.g., real or imaginary part)
def extract_500mhz_real(data):
    return data[3, 1] if data is not None else None

def extract_500mhz_imaginary(data):
    return data[3, 2] if data is not None else None

def extract_25ghz_real(data):
    return data[100, 1] if data is not None else None

def extract_25ghz_imaginary(data):
    return data[100, 2] if data is not None else None

def extract_50ghz_real(data):
    return data[-1, 1] if data is not None else None

def extract_50ghz_imaginary(data):
```

```
    return data[-1, 2] if data is not None else None

#phantom and tumour parameters
phantom_center = (9.5, 9.5)
phantom_radius = 9.5
tumour_center = (9.1, 9.1)
tumour_radius = 2

# Folder path
folder_path = '/content/drive/My Drive/Colab Notebooks/Phantom_22.09.24/
    with skin average right'
files = glob.glob(os.path.join(folder_path, "*.prn"))

#subplots
fig, axes = plt.subplots(3, 2, figsize=(14, 18))
plt.subplots_adjust(hspace=0.4, wspace=0.3)

#circular mask
def create_circular_mask(xi, yi, center, radius):
    mask = (xi - center[0])**2 + (yi - center[1])**2 <= radius**2
    return mask

# heatmap with phantom mask
def plot_heatmap(extract_func, ax, title, cmap_label):
    x_positions = []
    y_positions = []
    permittivity_values = []

    for file in files:
        x, y = extract_coordinates(os.path.basename(file))
        data = read_data(file)
        if data is not None:
```

```
            permittivity = extract_func(data)
            if permittivity is not None:
                x_positions.append(x)
                y_positions.append(y)
                permittivity_values.append(permittivity)

    if len(permittivity_values) > 0:
        x = np.array(x_positions)
        y = np.array(y_positions)
        z = np.array(permittivity_values)

        xi = np.linspace(0, 19, 1300)
        yi = np.linspace(0, 19, 1300)
        xi, yi = np.meshgrid(xi, yi)

        #  Rbf - radial basis function interpolation
        rbf = Rbf(x, y, z, function='multiquadric', smooth=0.1)
        zi = rbf(xi, yi)

        # circular phantom
        phantom_mask = create_circular_mask(xi, yi, phantom_center,
            phantom_radius)
        zi_masked = np.ma.masked_where(~phantom_mask, zi)

        heatmap = ax.pcolormesh(xi, yi, zi_masked, shading='auto', cmap='
            jet')
        ax.set_title(title, fontsize=16)
        ax.set_xlabel('X Position', fontsize=14)
        ax.set_ylabel('Y Position', fontsize=14)
        ax.scatter(x, y, color='grey', s=0.5)
        ax.set_xlim(0, 19)
        ax.set_ylim(0, 19)
```

```
113
114         # Adding the tumour and phantom circle
115         tumor_circle = Circle(tumour_center, tumour_radius, color='black',
                fill=False, linewidth=2, linestyle='dashed')
116         ax.add_patch(tumor_circle)
117
118         phantom_circle = Circle(phantom_center, phantom_radius, color='
               black', fill=False, linewidth=2, linestyle='dashed')
119         ax.add_patch(phantom_circle)
120
121         cbar = fig.colorbar(heatmap, ax=ax)
122         cbar.set_label(cmap_label,fontsize=16)
123
124 # Plots-heatmaps
125 plot_heatmap(extract_500mhz_real, axes[0, 0], '900 MHz Real Permittivity',
        'Real Permittivity')
126 plot_heatmap(extract_500mhz_imaginary, axes[0, 1], '900 MHz Imaginary
    Permittivity', 'Imaginary Permittivity')
127 plot_heatmap(extract_25ghz_real, axes[1, 0], '25 GHz Real Permittivity', '
    Real Permittivity')
128 plot_heatmap(extract_25ghz_imaginary, axes[1, 1], '25 GHz Imaginary
    Permittivity', 'Imaginary Permittivity')
129 plot_heatmap(extract_50ghz_real, axes[2, 0], '50 GHz Real Permittivity', '
    Real Permittivity')
130 plot_heatmap(extract_50ghz_imaginary, axes[2, 1], '50 GHz Imaginary
    Permittivity', 'Imaginary Permittivity')
131
132
133 plt.show()
```